APPENDIX - PAPERS A - E

Paper A.

Arrays of Distributed-Bragg-Reflector Waveguide Lasers at 1536 nm in Yb/Er-co-doped Phosphate Glass*

David L. Veasey, David S. Funk, Norman A. Sanford
Optoelectronics Division, National Institute of Standards and Technology,
325 Broadway, MC 815.04
Boulder CO 80303-3328, USA
Phone: (303) 497-5952
E-mail: veasey@boulder.nist.gov dfunk@boulder.nist.gov
sanford@boulder.nist.gov

Joseph S. Hayden
Schott Glass Technologies, Inc.
400 York Ave., Duryea, PA 18642, USA
Phone: (717) 457-7485 ext 351
E-mail: jhayden@sp230l.attmail.com

We have successfully demonstrated an array of monolithic, single-frequency distributed-Bragg-reflector (DBR) waveguide lasers operating near 1536 nm wavelengths. The lasers were fabricated by forming waveguides in Yb/Er-co-doped phosphate glass by ion exchange. The slope efficiency for each laser as a function of launched pump power is 26 % and the thresholds occur at 50 mW of launched pump power. An output power of 80 mW was achieved with 350 mW of coupled pump power. Each laser exhibits stable operation on a single longitudinal mode and all have linewidths less than 500 kHz. A comb of waveguides with varying effective indices allows the selection of wavelength using a single-period grating.

A1
15

We describe in this letter the first reported monolithic, single-frequency distributed-Bragg-reflector (DBR), waveguide lasers in Yb^{3+}/Er^{3+}-co-doped phosphate glass. Over the past several years, the growth in the demand for bandwidth generated by new telecommunication services, cable television (CATV), and data communication has driven the rapid development of wavelength division multiplexing (WDM) where information is simultaneously transmitted on several different wavelengths in the same optical fiber channel. The development of WDM, systems has placed demands on laser sources that are difficult to meet using existing technologies such as semiconductor distributed feedback (DFB) lasers. Issues of concern for such systems include wavelength selectivity, wavelength stability over laser lifetime, tunability, process yield, power limitations, and costs.

Integrated, single-frequency, solid-state lasers using the Er^{3+} ion offer a very promising and competitive alternative to DFB lasers for use in future WDM communications systems and for CATV. Several demonstrations of the waveguide and fiber laser technology have been discussed in the literature.[1-5] One primary advantage of solid-state waveguide lasers is that they offer the possibility for arrays of lasers operating on many wavelengths on a single glass chip. Rare-earth-doped waveguide lasers can also provide kilohertz linewidths with high radiance, low noise, and easy coupling to optical fibers.[3,4,6]

Single-transverse-mode waveguides at 1535 nm wavelength were fabricated in a commercially available phosphate alkali glass that was co-doped with 0.99×10^{20} Er^{3+} ions/cm^3 and 3.97×10^{20} Yb^{3+} ions/cm^3.[7,8] Phosphate glass is a very good host material for ytterbium and erbium ions since the sensitization efficiency is nearly unity and large

doping concentrations are possible before the onset of concentration quenching.[9] The guides were formed by ion exchange of K^+ for Na^+ using line apertures 3 to 8 μm wide etched in a 200 nm thick aluminum mask layer. The exchange time was 4 hours in an aluminum crucible containing molten KNO_3 at 375 °C. Inspection of the samples using refractive near-field scanning after the ion exchange revealed that the regions of the glass surface corresponding to the location of the mask openings had become recessed by approximately 1 μm during the exchange process.[10] The mechanism behind the etching of the glass during the exchange is currently under investigation, and we think it is caused by residual water in the hygroscopic nitrate melt.[9] The surface quality of the glass in the recessed regions, as observed using a 1000x nomarski contrast microscope, appears identical to the original surface of the glass and apparently does not cause significant scattering losses.

The waveguide end faces were polished perpendicular to the channels. The length of the waveguides prior to the grating fabrication step was 2.2 cm. Measurements of the waveguide mode-field dimensions showed that a single transverse mode was supported in each of the waveguides. For the guide formed with the 6.5 μm mask aperture, the 1/e full-widths of the mode-field intensity were 16 μm wide by 11 μm deep at 1.54 μm wavelength. It supported multiple transverse modes at the 977 nm pump wavelength. However, when the device was lasing, the pump energy was confined primarily within the lowest order transverse mode, which had 1/e dimensions of 13 μm wide by 9.5 μm deep. All measurements of the intensity profile are within an estimated experimental error of ± 10%.

A DBR surface relief grating was fabricated holographically in a 0.5 μm thick layer of Shipley 1805[8] photoresist using a 90° corner that split a collimated laser beam into tw beams.[11] The corner was mounted on a rotation stage so that the angle of the two beams could be varied. One surface of the corner was a mirror, and the other surface was a vacuum chuck for holding the sample. Light from a 457.8 nm Ar-ion laser was spatially filtered by focusing through a 15 μm pinhole using a 20x objective lens.

The beam was collimated using a 76 mm diameter lens with a 350 mm focal length. The exposure angle was set to write a grating with a pitch of Λ = 507.8 nm. For a waveguide with estimated effective index of 1.515 ± 0.003, this pitch should provide laser operation at λ =1538.6 nm ± 3 nm.. The exposure time for the photoresist was 18 s with 3.85 mW incident in each arm on the 0.44 cm^2 exposed region (0.8 cm long x 0.55 cm wide). The grating was developed in undiluted Shipley CD-30[8] developer. During the development, the diffraction of light from a 632.8 nm HeNe laser was monitored.[12] When the first-order diffracted power reached a peak, the grating was removed, rinsed, and dried.

Before transferring the photoresist pattern into the glass by Ar-ion sputtering, we deposited 40 nm of Cr on the surface with the specimen inclined 60° to the electron-beam evaporation source. Mounting the specimen in this way causes Cr to accumulate only on the tops of the grating lines and not in the grooves, thus providing a durable etch mask. We etched the grating in the glass for 20 minutes using a reactive ion etching system with a 6.67 Pa (50 mTorr) Ar-ion plasma. The low-pressure plasma created a large self-bias voltage of 1700 V when running at 365 W of coupled power with frequency 13.5 MHz. The electrode spacing was 3.2 cm. After etching, the sample was cleaned ultrasonically in photoresist stripper at 85 °C. Figure 1 is an illustration of the completed DBR laser

array. An atomic f rce microscope micro-graph of a typical grating etched in this type of phosphate glass can b found in reference [11].

The waveguide laser cavities were formed by placing a thin, highly reflecting (R=99.9% at 1540 nm, R=15% at 977 nm) dielectric mirror on the pump input facet. The mirror was held in place by a spring clip, and index-matching fluid was used between the mirror and the waveguide facet. The DBR grating was used as the laser output coupler. We tested the laser by coupling light from a Ti:Al_2O_3 laser tuned to a wavelength of 977 nm using a 4x objective lens with a numerical aperture of 0.1. The launching efficiency was estimated to be between 65 and 71 percent. To determine the launching efficiency we measured the Fresnel reflectance of the input mirror, the loss of the launching objective, and the excess coupling loss. Figure 2 shows the laser output power as a function of launched pump power and the spectrum of the laser. The waveguide diffusion aperture for this waveguide was 8 μm. The slope efficiency as a function of launched pump power is calculated to be 26 percent when we take the coupling factor to be 71 percent.

We estimated the reflectance of the grating using the simplified laser formula derived from the theory of Rigrod:[13]

$$\frac{P_1}{P_2} = \frac{1-R_1}{1-R_2}\sqrt{\frac{R_2}{R_1}} \qquad (1),$$

where P_1 is the output power at the grating end and P_2 is the output power at the end opposite the grating. R_1 is the grating reflectance and R_2 is the reflectance of the attached mirror. We used two mirrors with reflectances of 80 and 90 percent for R_2. For both cases we calculated the grating reflectance, R_1, to be 65 percent.

A3

To investigate the longitudinal mode structure of the laser we coupled the laser output into an optical fiber scanning Fabry Perot interferometer with a free spectral range of 124 GHz. Figure 3 shows that the laser operated on a single longitudinal mode when the coupled pump power did not exceed 300 mW. The laser was robustly single frequency with TE polarization, and no mode hopping was observed. The inset in Figure 3 shows that a second longitudinal mode appeared when the coupled pump power exceeded 300 mW. In this pump regime, the laser was unstable and exhibited mode hopping, single-frequency operation, and dual-frequency operation. By measuring the frequency spacing between the longitudinal modes we determined that the physical length of the laser cavity was 1.4 cm.

We measured the linewidth of the laser using a conventional self-heterodyne configuration with a 75 MHz frequency shift.[14] The path length difference between the two arms was 10 km corresponding to a linewidth resolution limit of 30 kHz for a gaussian line shape.[15] Optical isolators were used in both arms to prevent optical linewidth narrowing due to feedback; however, the output end of the laser was not beveled. Figure 4 shows the self-heterodyne spectrum. The laser linewidth we obtained from this measurement was 500 kHz.

Finally, we measured the laser wavelengths of other waveguides on the chip using an automatic spectrum analyzer with a resolution of 0.1 nm. Seven of the eleven waveguides on the chip exhibited laser oscillation. The waveguides formed through the smaller apertures did not achieve threshold because the smaller mode volumes caused a reduction of the gain such that the 45 percent transmittance loss of grating could not be overcome. Figure 5 shows the change in wavelength trend as we scanned the

waveguides. The wavelength increases as the diffusion aperture width increases, which is consistent with increasing effective index as the aperture width increases.

In conclusion, we have demonstrated an array of high power, robustly single-frequency, integrated, DBR waveguide lasers operating near 1536 nm wavelength. The slope efficiencies of the lasers are 26 percent based on launched pump power, and the threshold is less than 50 mW when pumped at a wavelength of 977 nm. The linewidths of the lasers were measured to be 500 kHz, and the outputs were linearly polarized in a TE mode. We are currently investigating the temperature stability of the lasers and the relative intensity noise (RIN). We expect that with diode laser pumping, the RIN will be similar to other results presented for single-frequency fiber lasers and will fall below -150 dB/Hz above 10 MHz. We anticipate that the output power and efficiency will increase and the threshold power will decrease when the grating reflectance is increased. This is possible with only minor adjustments to the grating fabrication process. Further improvements will also be realized by directly coating the high reflector onto the waveguide end facets. We have shown that lasers with several output wavelengths can be integrated on a single glass substrate. This demonstration shows that stable, multi-wavelength, WDM sources with wavelengths falling on the International Telecommunications Union (ITU) grid can be realized by writing several gratings of varying period in Yb/Er-co-doped glass waveguides formed by ion exchange.

A7

References

[1]T. Kitagawa, F. Bilodeau, B. Malo, S. Theriault, J. Albert, D.C. Johnson, K.O. Hill, K. Hattori, and Y. Hibino, Electron. Lett., 30, 1311 (1994).

[2]A. Yeniay, J.-M.P. Delavaux, J. Toulouse, D. Barbier, T.A. Strasser, and J.R. Pedrazanni, IEEE Photonics Technol. Lett. 9, 1099 (1997).

[3]J.T. Kringlebotn, J.-L. Archambault, L. Reekie, J.E. Townsend, G.G. Vienne, and D.N. Payne, Electron. Lett. 30, 972 (1994).

[4]W.H. Loh, B.N. Samson, L. Dong, G.J. Cowle, and K. Hsu, J. Lightwave Technol. 16, 114 (1998).

[5]G.J. Vossler, C.J. Brooks, and K.A. Winick, Electron. Lett. 31, 1162 (1995).

[6]T.Y. Fan, R.L. Byer, IEEE J. Quantum Electron. 24, 895 (1988).

[7] IOG-1 laser glass, Schott Glass Technologies, Inc., 400 York Avenue, Duryea, PA.

[8]Specific materials and process chemicals are reported only to make the process reproducible and are not endorsed by the U.S. Government. Other materials and chemicals may work as well or better.

[9]P. Fournier, P. Meshkinfam, M.A. Fardad, M.P. Andrews, and S.I. Najafi, Electron. Lett. 33, 293 (1997).

[10] B. Groebli, B. Gisin, N. Gisin and H. Zbinden, *Opt. Engineering*, 34, 2309 (1995), N. H. Fontaine and M. Young, "Refracted near-field scanning of fibers and waveguides," submitted to *J. Lightwave Technol.*

[11]D.L. Veasey, K.J. Malone, J.A. Aust, N.A. Sanford, and A. Roshko, Proc. 7th Eur. Conf. on Int. Opt. p. 579, Delft, (1995). J.B. Roman and K.A. Winick, Appl. Phys. Lett. 61, 2744 (1992).

[12]L. Li, M. Xu, G.I. Stegeman, C.T. Seaton, SPIE Proc. 835, 72 (1987).

[13] W.W. Rigrod, J. Appl. Phys. 36, 2487 (1965).

[14]D.H. McMahon, W.A. Dyes, J. Lightwave Technol. 6, 1162 (1988).

[15] J.W. Goodman, *Statistical Optics*, Wiley&Sons, 1985, p. 168.

(A 8)

22

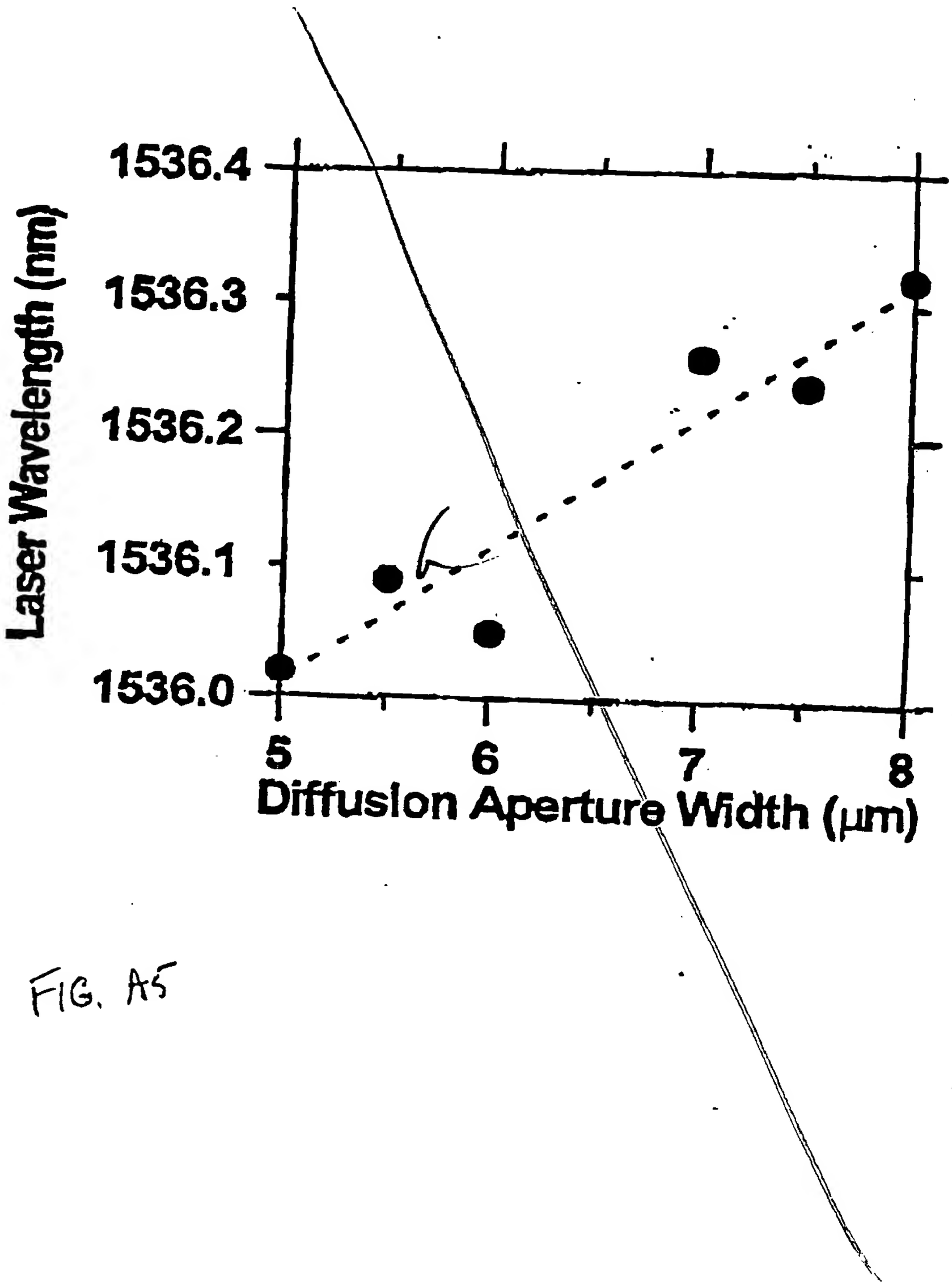
1536.4
1536.3
1536.2
1536.1
1536.0
Laser Wavelength (nm)
5
6
7
8
Diffusion Aperture Width (μm)

FIG. A5

Paper B

170 mW cw at 1540 nm from an erbium/ytterbium co-doped glass waveguide laser

D. S. Funk, D. L. Veasey, P. M. Peters and N. A. Sanford
National Institute of Standards and Technology,
Optoelectronics Division, 814.04,
325 Broadway, Boulder, CO 80303
phone: (303)-497-3289 fax: (303)-497-3387
dfunk@boulder.nist.gov

J. S. Hayden
Schott Glass Technologies, Inc., R&D-Materials Group,
400 York Avenue, Duryea, PA 18642
phone: (717)-457-7485 fax: (717)-457-3438
jhayden@sg230L.attmail.com

Compact solid state lasers based on the 1.5 μm Er^{3+} transition hold promise as sources for optical fiber communication systems. Yb^{3+} is commonly used as a sensitizer in Er^{3+} lasers because it has a much larger absorption cross section near 980 nm than Er^{3+}, and it efficiently transfers its excited state energy to the upper level of the Er^{3+} laser. The Er^{3+}\Yb^{3+} glass waveguide laser, in particular, has several advantages over lasers in Er^{3+}-doped or Er^{3+}/Yb^{3+}-co-doped glass fiber and bulk crystalline or glass hosts. Ion-exchanged waveguides can be fabricated in glasses with large ytterbium concentrations (~5-15 %) which allows the devices to be substantially shorter than fiber lasers. This results in lower polarization and output power noise, caused by thermal and mechanical stress-induced birefringence, and a smaller device volume. Short (~ 1-2 cm) laser cavities are also of interest because of the potential for realizing high pulse repetition rate (GHz), passively mode-locked lasers. Unlike bulk devices, waveguide lasers can be designed to operate in a single transverse mode independent of the operating power or pump laser transverse mode profile, and do not require the alignment of bulk mirrors. In addition, the mode field sizes in waveguides can be designed to closely match those of optical fiber for efficient coupling with fiber optic systems. One disadvantage of Er^{3+}/Yb^{3+} glass waveguide lasers, up to this point, has been the relatively low output powers (up to a few milliwatts[1-4]) available from these devices. Increased output power will greatly expand the utility of these devices. This paper describes a cw Er^{3+}/Yb^{3+}-codoped phosphate glass waveguide laser which has produced 168 mW of output power at around 1540 nm for 611 mW of launched pump power at 979 nm.

Waveguides were fabricated in a commercially available phosphate glass.[4] The glass was co-doped with 1.15 wt % Er_2O_3 (0.99×10^{20} ions/cm^3) and 4.73 wt % Yb_2O_3 (3.97×10^{20} ions/cm^3). Waveguides were formed by K^+-Na^+ exchange through a 200 nm thick Al mask layer with channel apertures ranging from 3 to 8 μm in width. The exchange occurred in a KNO_3 melt at 375 °C for 4 hours in an Al crucible. The laser results reported here are for a 6.5 μm wide mask aperture. Inspection of the samples after the ion exchange process revealed that the regions of the glass surface corresponding to the location of the mask openings had become recessed by one to two microns during the exchange process. The widths of the etched channels were close to the widths of the mask apertures and uniform in width and depth. The mechanism behind the apparent etching of the glass during the exchange process is currently under investigation.

The refractive index as a function of position within the exchanged sample was analyzed using a refractive near-field scanning method.[5] Figure 1 shows the index depth profile at the center of the waveguide formed with the 6.5 μm mask aperture for a wavelength of 633 nm. This method allows the relative position and absolute index values to be determined with an accuracy of 0.7 μm and 0.001, respectively.

The transverse modes of the waveguides were characterized by coupling light at the wavelength of interest into one end of the waveguide and imaging the light emerging from the other end onto a calibrated infrared camera. The uncertainty of the mode dimensions determined using this method are ~10 %. The device supported a single transverse mode at 1.54 μm having dimensions of 14.5 μm wide by 7.5 μm deep (measured at the 1/e points). The waveguide supported multiple transverse modes at 980 nm. However,

B1

when the device was lasing, the pump energy was confined primarily within the lowest order transverse mode which had dimensions of 6.4 μm wide by 3.6 μm deep.

The device was pumped with a Ti^{3+}:sapphire laser. The waveguide laser cavities were formed by placing thin dielectric mirrors on the polished waveguide end faces. The mirrors were held in place by small spring clips, and index matching oil was used between the mirror and waveguide end face to reduce losses. The pump laser was launched through one of the mirrors with a 4X microscope objective. The laser output and unabsorbed pump were collimated with a 16X microscope objective and separated using filters. The laser cavity was 20 mm in length. The mirror through which the pump was launched had reflectivities of >99.9 % and 15 % at 1536 and 980 nm, respectively. The output coupler had a reflectivity of 80 % at 1536 nm and transmitted 85 % of the incident pump power. Neither the waveguide length nor the cavity output coupling has been optimized. The launching efficiency was estimated to be ≤ 71 %, including losses due to the transmission of the input mirror and launching objective. The laser output power characteristics for two different pump wavelengths are illustrated in Figure 2. When pumped at 979 nm, the launched pump power threshold was 51 mW. A maximum output power of 168 mW was obtained for 611 mW of launched 979 nm pump power. A lower threshold could be obtained by tuning the pump laser off of the Yb^{3+} absorption peak. For a pump wavelength of 960 nm, the threshold was 23 mW. The slope efficiency for both pump wavelengths was ~28 %.

Using the broad band cavity described above, the Er^{3+}/Yb^{3+} laser usually operated at several wavelengths simultaneously. A typical laser spectrum showing simultaneous operation at 1536.0, 1540.7, and 1544.8 nm is depicted in Figure 3. The wavelength(s) of operation could be shifted by passing some of the collimated 1.5 μm laser output through a prism and reflecting it back through the prism and into the waveguide using a dielectric mirror. This formed a weakly-coupled, external cavity. By rotating the prism, it was possible to produce wavelengths ranging from 1536 to 1595 nm.

A common feature of many three level rare-earth lasers is sustained relaxation oscillations which can be caused by small fluctuations in the pump laser power. Fluctuations in output power at frequencies ranging from ~ 0.5 to 1.5 MHz were observed in this laser. The amplitude of the fluctuations decreased with pump power. Figure 4 shows the output power as a function of time for pump power levels just above threshold and 9.4 times threshold. At the low pump power, the output power fluctuations of ~ 30 % (peak to peak) of the average power were observed. At the high pump power, the fluctuations decreased to ~ 5 % (peak to peak) of the average power. The Ti^{3+}:sapphire pump laser exhibited output power fluctuations of ~ 2-3 %. Using a diode laser as the pump source should result in much quieter operation of the Er^{3+} laser.

Output powers exceeding 160 mW at 1.5 μm are now available from glass waveguide lasers fabricated using a simple thermal ion exchange process. Improvements in the waveguide fabrication process to optimize the waveguide geometry (such as incorporating a field assisted ion exchange and fabricating buried waveguides), as well as adjustments in the cavity length and output coupling, should improve the performance of these devices.

---

[1] J. E. Román, M. Hempstead, W. S. Brocklesby, S. Nouh, J. S. Wilkinson, P. Camy, C. Lerminiaux and A. Béguin, "Ion-exchanged Er/Yb waveguide laser at 1.5 μm pumped by a laser diode," *Electron. Lett.*, vol. 31, p. 1345, 1995.

[2] G. L. Vossler, C. J. Brooks and K. A. Winick, "Planar Er:Yb glass ion exchange waveguide laser," *Electron. Lett.*, vol. 31, p. 1162, 1995.

[3] D. Barbier, J. M. Delavaux, R. L. Hyde, J. M. Jouanno, A. Kervorkian and P. Gastaldo, "Tunability of Yb/Er integrated optical lasers in phosphate glass," *Amplifiers and their Applications, 1995 Tech. Dig. Serv.*, Davos: Switzerland, vol. 18, paper PD3.

[4] J. Amin, D. L. Veasey, N. A. Sanford and J. S. Hayden, "Waveguide lasers by ion-exchange in Er-doped glass," in *Rare-Earth-Doped Devices, Proc. SPIE*, vol. 2996, p. 135, 1997.

[5] IOG-1 laser glass, Schott Glass Technologies, Inc., 400 York Avenue, Duryea, PA. The IOG-1 tradename is used to allow the reader to reproduce the experiment and does not imply endorsement by the National Institute of Standards and Technology.

[6] B. Groebli, B. Gisin, N. Gisin and H. Zbinden, "Measuring refractive index profiles of integrated $LiNbO_3$ waveguides," *Opt. Engineering*, vol. 34, p. 2309, 1995.

(62)

25

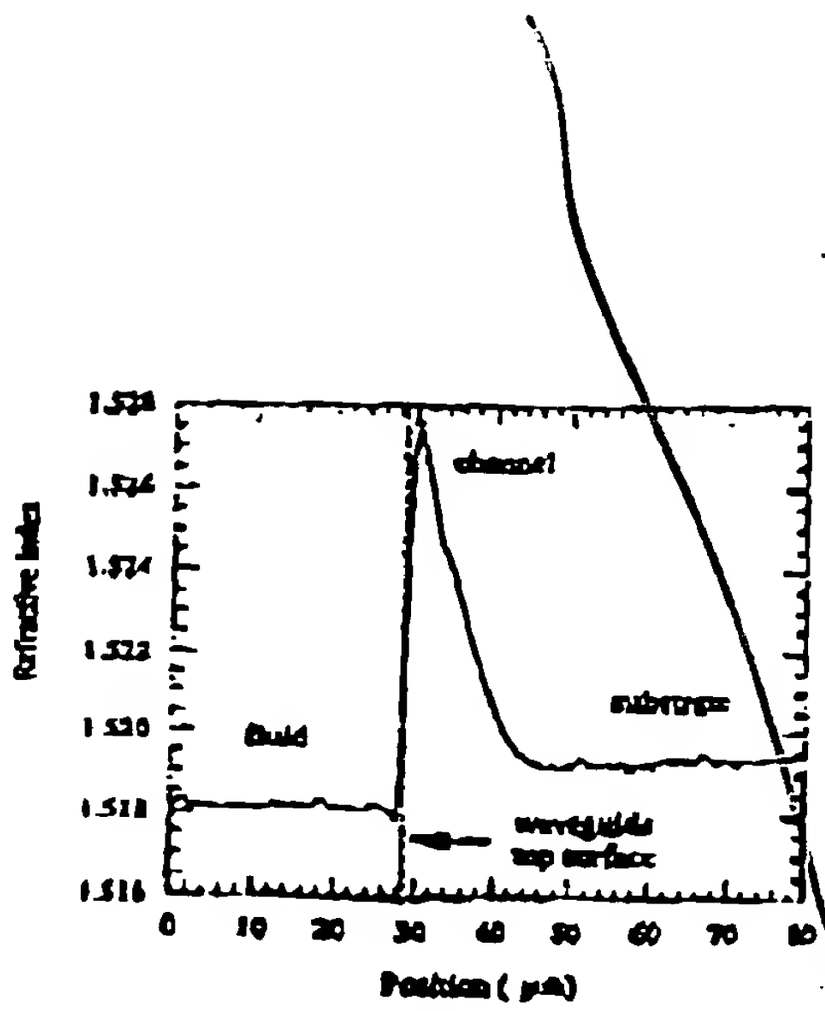

Fig B1. Refractive index profile at 633 nm of an Er^{3+}/Yb^{3+} phosphate glass waveguide, obtained using a refracted near-field scanning method.

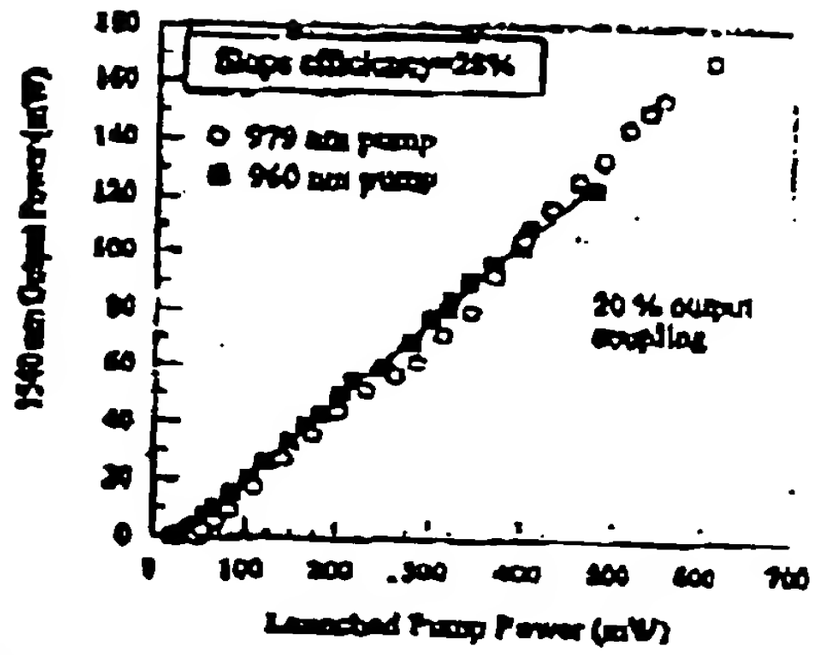

Fig B2. 1540 nm output power as a function of pump power for a 20 mm long Er^{3+}/Yb^{3+} waveguide laser. Curves are shown for two different pump wavelengths.

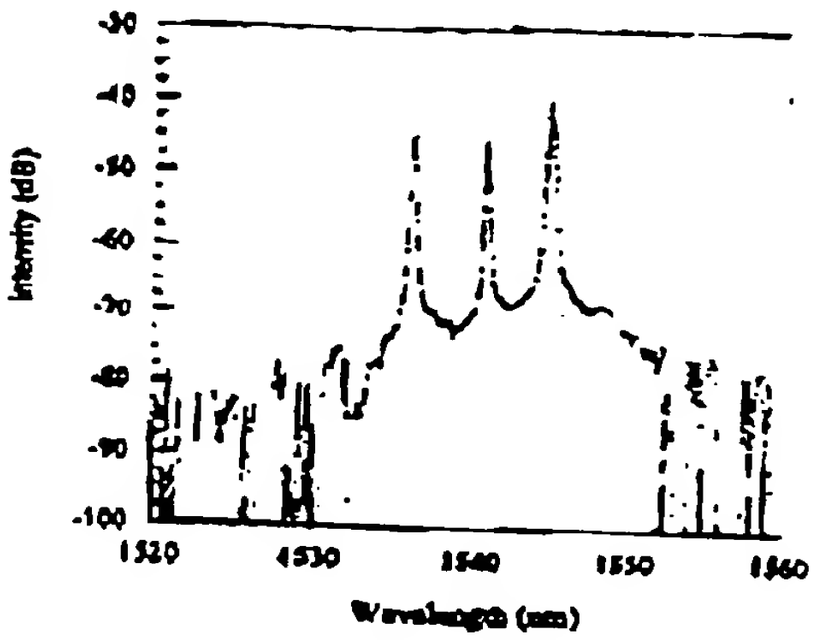

Fig B3. Laser output spectrum of an Er^{3+}/Yb^{3+} waveguide laser spectrum for 106 mW of launched pump power.

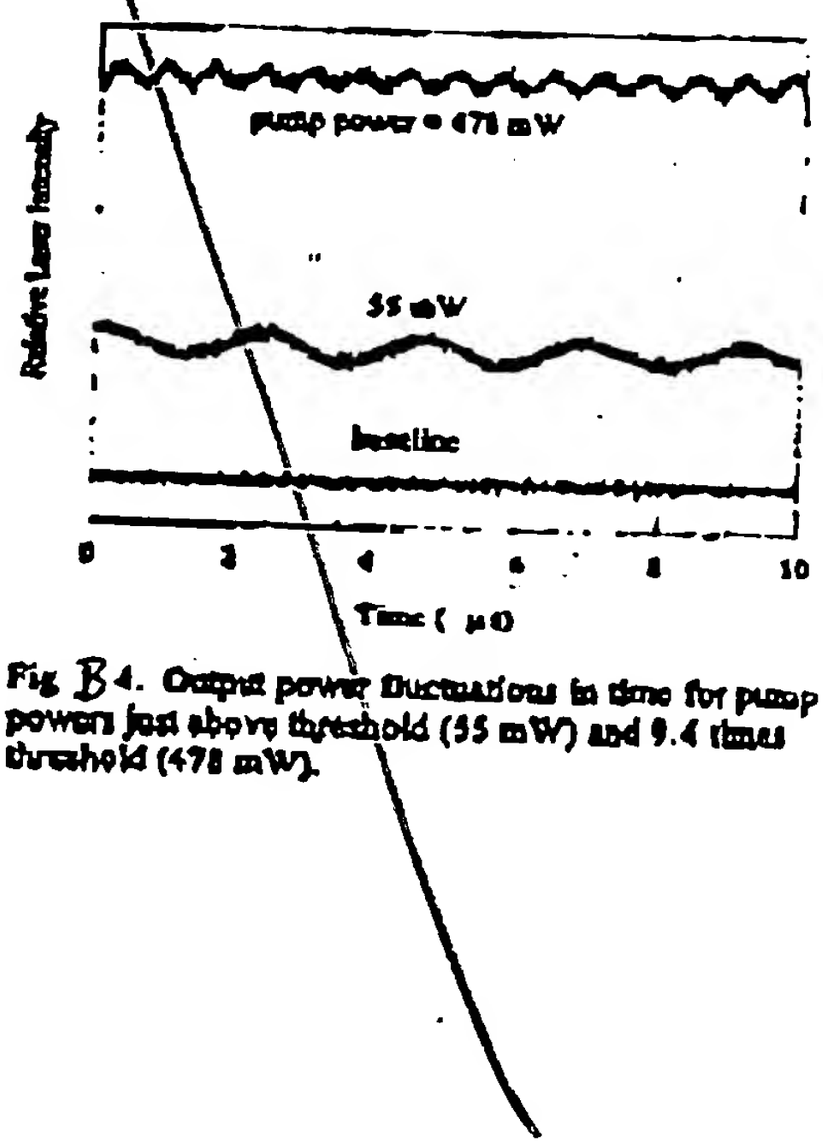

Fig B4. Output power fluctuations in time for pump powers just above threshold (55 mW) and 9.4 times threshold (478 mW).

Paper C.

Ion-exchanged Er^{3+}/Yb^{3+} glass waveguide lasers in silicat glasses[1]

P. M. Peters, D. L. Veasey, D. S. Funk and N. A. Sanford
Optoelectronics Division, 815.04, National Institute of Standards and Technology, 325 Broadway, Boulder, CO 80303

S. N. Houde-Walter
The Institute of Optics, University of Rochester, Rochester, NY 14627

J. S. Hayden
R&D-Materials Group, Schott Glass Technologies, Inc., 400 York Avenue, Duryea, PA 18642

Waveguide lasers and amplifiers in glasses codoped with Er^{3+} and Yb^{3+} are promising candidates for compact multifunctional devices operating near 1.5 μm. The large gain bandwidth resulting from the inhomogeneously broadened glass host makes these devices ideal for narrow-line sources useful in wavelength division multiplexing applications. In addition, due to the short cavity lengths, these waveguide lasers offer the possibility of high repetition rate (GHz) mode-locked lasers using semiconductor saturable absorbers. Such lasers would be ideal as sources for soliton communications systems. Other applications requiring an eye-safe wavelength, such as remote sensing and range finding, could benefit from compact, high power cw or Q-switched waveguide laser sources based on these materials. Additionally, optical amplifiers offering gain in the range 1530 to 1550 nm may be realized.[1]

It is known that the Er^{3+} concentration must be kept relatively low (~ 1 wt %) in these devices in order to reduce the deleterious effects of cooperative upconversion. However, the concentration of sensitizing Yb^{3+} is not limited due to any ion-ion interaction, and is expected to have a significant effect on device performance. Various authors have investigated this problem theoretically.[2,3] In this paper we report experimental results for waveguide lasers fabricated by K^+-Na^+ ion exchange in silicate glasses with Yb^{3+}:Er^{3+} ratios of 3:1, 5:1, and 8:1. In addition, we show how it is possible to increase the signal mode volume and optimize the pump-signal overlap through judicious choice of laser host material and ion exchange processing parameters. The result is an Er^{3+}/Yb^{3+} waveguide laser producing as much as 19.6 mW at 1.54 μm with 398 mW of launched pump power at 974.5 nm.

The devices were fabricated in a commercially available laser glass.[4] The glass is a phosphorus-free, mixed-alkali, zinc silicate glass. Nominally, all three glasses were doped with 1 wt% Er_2O_3 (0.85×10^{20} cm^{-3}) and the glasses designated NIST10A, NIST10C, and NIST10E contain Er^{3+}:Yb^{3+} ratios of 3:1 (2.47×10^{20} Yb^{3+} ions cm^{-3}), 5:1 (4.16×10^{20} cm^{-3}), and 8:1 (6.83×10^{20} cm^{-3}), respectively. The results reported were obtained by ion exchange through 3 μm apertures in 150 nm thick Al mask layers. The ion exchange was carried out in a melt of 100% KNO_3 for 14 hours at 400 °C.

[1] Contribution of the U.S. Government, not subject to copyright.

C1

The optical modes of the waveguides at the signal wavelength were evaluated by coupling a 1.5 μm LED into a waveguide while the output was imaged onto an infrared camera. The waveguides supported a single transverse mode of dimensions 20.5 ± 2.1 μm wide by 11.5 ± 1.2 μm deep (measured at the 1/e points) at the signal wavelength. Since the host glass is a mixed alkali glass which contains potassium, the introduction of additional potassium by the ion exchange process leads to a very small index change. As a result the optical mode is not tightly confined. Although the waveguides supported multiple transverse modes at the pump wavelength, an examination of the pump mode while the device was lasing showed that only the lowest-order mode was excited. The result is excellent overlap between the pump and signal modes. The pump mode measured 15.2 ± 1.5 μm wide by 7.0 ± 0.7 μm deep.

Waveguide losses were estimated at 860 nm, away from the broad Yb^{3+} absorption peak. Cutback measurements performed on samples prepared identically to the laser sample indicated an average waveguide loss of 0.25 ± 0.11 dB/cm for NIST10A, 0.32 ± 0.08 dB/cm for NIST10C, and 0.66 ± 0.12 dB/cm for NIST10B. The coupling efficiency for the pump light was determined by measuring the pump throughput at 860 nm and correcting for losses from the input and output optics, as well as waveguide loss using the above reporteded loss figures. Coupling efficiencies typically fell between 50% and 70%. The coupling efficiency was assumed to be identical at 860 nm and 975 nm.

For laser characterization, dielectric mirrors were attached to the polished end facets of the waveguide laser sample with index matching fluid and held in place by a small clip. The input mirror had a reflectance at 1536 nm of 99.9% and a transmittance at the pump wavelength of >90%. Various output couplers with reflectances ranging from 60 to 98% were used. All output couplers were also transmissive at the pump wavelength. The waveguide devices were pumped by a Ti:sapphire laser operating at 974.5 nm, which is the peak of the Yb^{3+} absorption spectrum in this glass host. Pump light was coupled into the waveguide with a 4X (0.10 NA) microscope objective, and the output signal light was collected by a 20X objective. For signal power measurements, the output from the waveguide was focused onto an InGaAs power meter.

The laser performance was investigated as a function of device length as well as output coupler reflectance. Figure 1 shows a plot of laser signal power vs. launched pump power for two different output couplers, for a 1.68 cm long device fabricated in the glass with 5 Yb^{3+} per Er^{3+} ion. The slope efficiencies and laser thresholds were determined by fitting a line to the laser data. The lowest threshold was achieved when using a 98% reflector as output coupler. This device lased with a launched pump power threshold of approximately 59 mW. The slope efficiency of this device was 2.0% with respect to launched pump power. The highest slope efficiency was realized with a 70% reflector used as an output coupler. In this case, a slope efficiency of 6.5% was achieved with a launched pump power threshold of 86 mW. For a launched pump power of 398 mW, this laser produced 19.6 mW of output power.

A plot of slope efficiency vs. output coupler reflectance for each host glass appears in Figure 2. Data for device lengths in each glass which were experimentally

determined to give the highest slope efficiency are plotted. Highest sl pe efficiency performance in each host is also compared in Table 1.

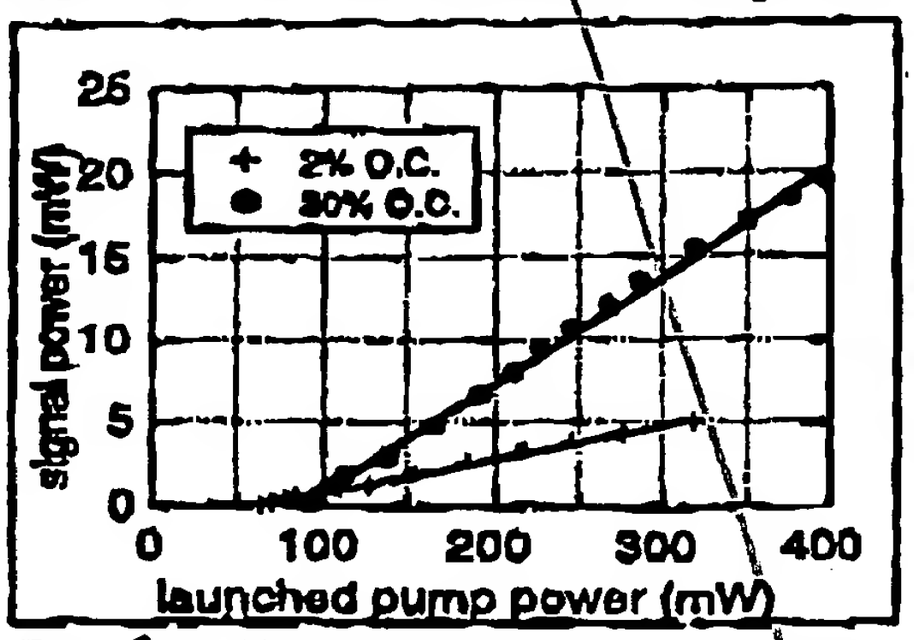

Fig. C1: Signal power vs. launched pump power for a 1.68 cm long device fabricated in the 5 Yb: 1 Er silicate glass.

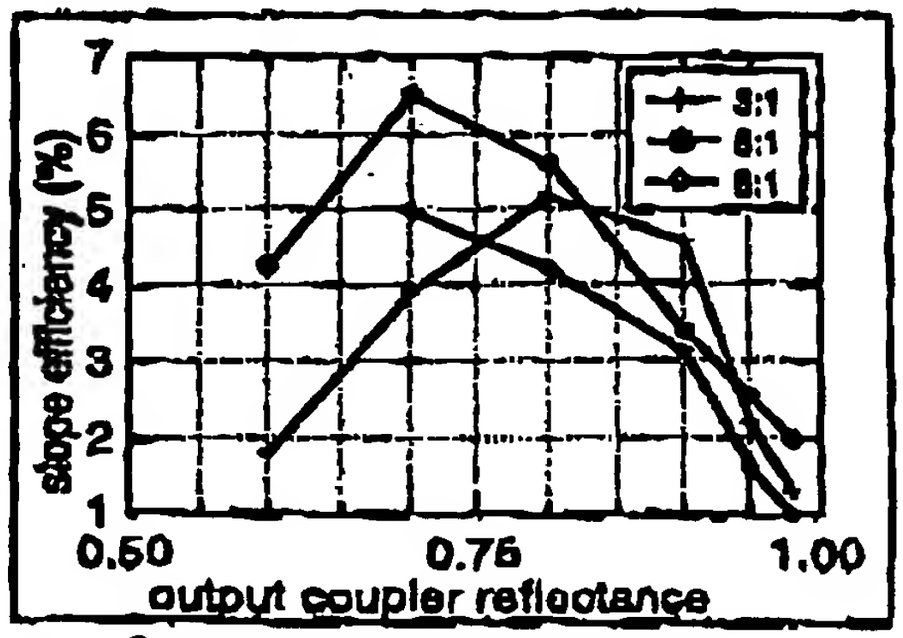

Fig C2: Slope efficiency vs. output coupler reflectivity for lasers fabricated in silicate glasses with different Yb:Er ratios.

Table 1: Performance data for highest slope efficiency devices fabricated in IOG10 silicate glass with different Yb^{3+}:Er^{3+} dopant ratios.

Yb^{3+}:Er^{3+}	Device length (cm)	Output coupler Reflectance (%)	Slope efficiency (%)	Launched pump threshold (mW)	Output with 400 mW pump (mW)
3:1	1.80	80	5.2	52	17.9
5:1	1.68	70	6.5	86	20.4
8:1	1.42	70	5.0	238	8.1

The experimental results indicate that the optimal dopant ratio is close to 5 Yb^{3+} for each Er^{3+}. Increasing the dopant ratio from 3:1 to 5:1 leads to an improvement in slope efficiency. Further increasing the dopant ratio to 8:1 does not improve the efficiency of the device, but does lead to a substantial penalty in pump power requirements. Recent efforts have been directed toward expanding the above results using a rigorous scalar model developed at NIST.[5] In addition, alteration of the potassium content of the host glass is being investigated as a way to adjust the modal volume and decrease pump threshold requirements.

---

[1] D. Barbier, M. Rattay, F. Saint André, G. Clauss, M. Trouillon, A. Kevorkian, J. -M. P. Delavaux and E. Murphy, IEEE Photon. Technol. Lett. 9, 315 (1997).
[2] F. Di Pasquale and M. Federighi, *IEEE J. Quantum Electron.* 30 2127 (1994).
[3] J. Nilsson, P. Scheer and B. Jaskorzynska, *IEEE Photon. Technol. Lett.* 6 383 (1994).
[4] IOG-10 laser glass, Schott Glass Technologies, Inc., 400 York Avenue, Duryea, PA. The IOG-10 tradename is used to allow the reader to reproduce the experiment and does not imply endorsement by the National Institute of Standards and Technology.
[5] D. L. Veasey, J. M. Gary and J. Amin, *Proc. SPIE* 2996 109 (1997).

Paper D

DRAFT DRAFT DRAFT

Yb/Er-codoped and Yb-doped Waveguide Lasers in Phosphate Glass*

David L. Veasey, David S. Funk, Philip M. Peters, Norman A. Sanford, Gregory E. Obarski, Norman Fontaine, Matt Young, Adele P. Peskin[a], Wei-chih Liu[b], S.N. Houde-Walter[c], Joseph S. Hayden[d]

National Institute of Standards & Technology
Optoelectronics Division, 325 Broadway, MC 815.04
Boulder, CO 80303-3328
E-mail: *veasey@boulder.nist.gov*

[a]National Institute of Standards & Technology
High Performance Systems and Services Division, 325 Broadway, MC 890.02
Boulder, CO 80303-3328
E-mail: *peskin@boulder.nist.gov*

[b]Rochester Theory Center
University of Rochester, Rochester, NY 14627
E-mail: weliu@pas.rochester.edu

[c]The Institute of Optics
University of Rochester, Rochester, NY 14627
E-mail: shw@optics.rochester.edu

[d]Schott Glass Technologies, Inc.
400 York Ave., Duryea, PA 18642, USA
E-mail: *jhayden@sg230l.attmail.com*

Abstract

We present experimental and theoretical results of our recent work on the development of waveguide lasers using rare-earth-doped phosphate glasses. An improvement has been achieved over previously reported waveguide laser results using the process of ion exchange in a commercially available Yb/Er-co-doped phosphate glass composition. We have demonstrated slope efficiencies near 30 percent with output powers approaching 200 mW for 1540 nm Fabry-Perot waveguide lasers. These lasers are continuously tunable over approximately 70 nm. In addition, Yb-doped Fabry-Perot waveguide lasers have been fabricated and tested. These lasers

---

operate near 1020 nm wavelength with slope efficiency of 67 %. We have also realized arrays of single-frequency distributed-Bragg-reflector waveguide lasers operating near 1.5 μm by etching a grating in ion-exchanged waveguides. Each laser in the array operates at a different wavelength. The slope efficiencies as a function of launched pump power are 26 % and the thresholds occur at approximately 50 mW of launched pump power. Temperature tuning of the wavelengths is also demonstrated.

1. Introduction

Waveguides in rare-earth-doped materials for lasers and amplifiers have been fabricated using a number of different methods. These include thermal and field-assisted ion exchange in bulk-doped silicate and phosphate glasses [1-8] and film deposition of several rare-earth-doped dielectric films that are formed into optical channel waveguides. Film deposition or formation methods include rf sputtering, [9-10] plasma-enhanced chemical vapor deposition,[11] flame hydrolysis,[12] ion implantation, [13] laser ablation, [14] and sol-gel deposition[15]. In this paper we restrict our discussion to waveguide lasers that are formed by ion-exchange in Yb/Er-codoped and Yb-doped phosphate glasses. We report on the development of the glass used to fabricate waveguide lasers and present recent measurement results for waveguide lasers. These measurements include slope efficiency and threshold, wavelength tuning, relative intensity noise and linewidth for single frequency distributed Bragg reflector (DBR) waveguide lasers. We conclude this paper with a brief discussion of a method to optimize the performance of waveguide lasers using a combination of experimental results and theoretical predictions.

2. Experimental Procedures

2.1 Development of Phosphate Glass

Perhaps the most critical step in the development of a robust waveguide laser technology is the design and realization of a suitable laser glass that supports ion exchange. The laser properties that must be engineered in the glass include the absorption and emission cross sections of the laser transition and the absorption and emission cross sections of the optical pump energy level. The spontaneous emission lifetimes must also be optimized for the laser and pump transition with the laser transition lifetime relatively long and the lifetime of the pump level as short as possible. Laser operation is also improved by reducing or eliminating the effects of cooperative upconversion. In codoped glasses, such as Yb/Er-codoped glass, the energy transfer efficiency from the sensitizing ion must be maximized. Yb codoping with Er in phosphate glasses can provide near unity sensitizing efficiencies. [16]

In addition to optimizing the rare-earth ion spectroscopic properties, the glass must have properties that allow the fabrication of channel waveguides. The most common way to form waveguides in bulk glasses is the process of ion exchange, where alkali ions in the glass are exchanged for ions with larger polarizability, thus causing an increase in the refractive index near the glass surface. Such a process requires that the starting glass contain alkali-oxide components such as Na_2O or K_2O. At the same time, the chemical treatments employed in conventional waveguide fabrication by lithographic technology demand that the host glasses offer chemical durability so that substrate surfaces are not degraded during the processing of devices.

A final requirement for waveguide laser glasses is that the rare-earth doping concentration be as large as possible to reduce cavity lengths and mode-volumes. It is

important that the doping concentration of the active rare earth ions be variable in a manner such that it can be altered without significantly altering the base glass matrix. Without this feature, each doping level can possibly represent a unique processing challenge as processing conditions may need to be adjusted to accommodate changes in base glass properties.

Based on the requirements set out above, we developed a glass that had both good laser and spectroscopic properties and good properties for ion exchange. The resulting glass composition, (with the commercial designation IOG-1 [17]), is given in mole percent oxide in Table 1. Al_2O_3 is added chiefly to increase durability since phosphate containing glasses with P_2O_5 content higher than 50 mole percent are normally react with molten salt baths and the other processing chemicals used in waveguide preparation (i.e. to remove ion diffusion barriers). The incorporation of a high total lanthanide content (denoted as R_2O_3 in Table 1) also contributes to enhanced chemical durability and allows for variation in active ion concentration with minimal impact on glass properties. The alkali oxide of choice is Na_2O since the sodium ion is known to be very mobile in glass and because sodium ion also exchanges well with potassium or silver for waveguide preparation.

All glasses were melted using high purity raw materials. Transition metal content in the glasses was estimated at 20 ppm Fe and less than 1 ppm for all other common transition metals. Lanthanum, erbium, and ytterbium rare earth compounds were selected to minimize the introduction of other lanthanide elements (less than 1000 ppm total). Melting and refining temperatures were typically 1250 to 1350 °C, with refining periods of 2 to 3 hours. Produced glass was cast into molds and annealed at 530 °C for 2 hours and cooled to room temperature at 30 °C/hr. Cast blocks were then used to prepare

characterization samples for refractive index, density and residual hydroxyl content at 3.0 μm and 3.333 μm. The measurements of index and density allowed calculation of estimated index values at lasing wavelengths and number density allowed calculation of estimated index values at lasing wavelengths and number density of rare earth input content using standard techniques. [18] Absorption at these wavelengths was monitored and held to levels of less than 1.0 cm^{-1} and 1.8 cm^{-1}, respectively.

2.2 Spectroscopic Measurements

Yb/Er-codoped and Yb-doped IOG-1 glass samples with were prepared for measurement of spectral absorption. Both glasses were doped with Yb concentration of 4×10^{20} cm^{-3} and the codoped sample contained 1×10^{20} cm^{-3} Er ions. The dimensions of the characterization samples were 9-mm thick, 21-mm tall and 10 mm wide. The absorption spectra were measured using an automatic spectrophotometer. The emission cross section spectrum for the erbium ions was calculated using the theory of McCumber [19] as applied by Miniscalco and Quimby [20] using the measured spectral absorption. The Yb emission cross section was obtained from measured spontaneous emission spectra and scaled to give the measured radiative decay rate. To measure the emission spectra, the samples were pumped at a wavelength of 974 nm and the spectra were recorded using a 0.3-m triple grating spectrometer.

The lifetime of the $^4I_{13/2}$ Er laser manifold in the codoped glass was measured in the limit of vanishing excitation power by chopping a 974 nm pump laser beam at 50 Hz using an acoustooptic modulator. The florescence decay near 1550 nm wavelength was observed to determine the 1/e lifetime. The lifetime of the $^2F_{5/2}$ Yb level was measured similarly by observing florescence decay near 974 nm.

2.3 Waveguide Laser Fabrication Process

Waveguide lasers were fabricated in Yb/Er-codoped and Yb-doped IOG-1 phosphate glasses. The Yb/Er glass was doped with 1.15 wt % Er_2O_3 (1.0×10^{20} ions/cm^3) and 4.73 wt % Yb_2O_3 (4.0×10^{20} ions/cm^3). For the Yb-doped laser, the glass was doped with 4.73 wt % Yb_2O_3 (4.0×10^{20} ions/cm^3). Waveguides were formed by K^+-Na^+ exchange through channel apertures ranging in width from 3 to 8 μm. The apertures were etched in a 200 nm thick Al mask layer. The exchange was performed in a crucible containing molten KNO_3 at 375 °C for 4 h. The Yb/Er laser results reported below are for a waveguide formed using a 6.5 μm mask aperture and the Yb laser results are for a 3 μm mask aperture.

A distributed Bragg reflector (DBR) surface relief grating was fabricated on a comb of eleven waveguides using a separate codoped specimen in a 0.5 μm thick layer of photoresist. A 90° corner split a collimated laser beam into two beams for a holographic exposure.[21] The exposure angle was set to write a grating with a period of $\Lambda = 507.8$ nm. For a waveguide with estimated effective index of 1.515 ± 0.003, this period was calculated to provide laser operation at $\lambda = 1538.6$ nm ± 3 nm. During the development of the photoresist, the diffraction of light from a 632.8 nm HeNe laser was monitored.[22] When the first-order-diffracted power reached a maximum, the grating was removed, rinsed, and dried.

Before transferring the photoresist pattern into the glass by Ar-ion sputtering, we deposited 40 nm of Cr on the surface with the specimen inclined 60° to the electron-beam evaporation source. Mounting the specimen in this way causes Cr to accumulate only on the tops of the grating lines and not in the grooves, thus providing a durable etch mask.

We etched the grating in the glass for 20 minutes using a reactive ion etching system with 6.67 Pa (50-mTorr) Ar-ion plasma. The low-pressure plasma created a large self-bias voltage of 1700 V when running at 365 W of coupled power with frequency 13.5 MHz. The electrode spacing was 3.2 cm. After being etched, the sample was cleaned ultrasonically in photoresist stripper at 85 °C. Figure 1 shows a schematic of a completed DBR laser array.

2.4 Waveguide and Laser Measurements

Several measurements were performed to determine the properties of the ion exchanged waveguides. The refractive index as a function of position within the sample was analyzed using the method of refractive near-field scanning. [23] The dimensions of transverse modes of the waveguides were measured by coupling light into one end of the waveguide and imaging the light emerging from the other end onto a calibrated infrared camera.

To test the Yb/Er-codoped Fabry-Perot lasers (lasers with no etched gratings), we typically pumped the waveguides using a tunable Ti: Al2O3 laser. Figure 2 shows a schematic of the laser measurement setup. Placing broadband dielectric mirrors on the polished waveguide end faces formed the laser cavities. The mirrors were held in place by small spring clips with index matching oil between the end facet and the mirror. The pump laser light was launched through one of the mirrors with a 4X microscope objective. The laser output and unabsorbed pump light were collimated with a 16X microscope objective and separated using filters. The mirror through which the pump light was launched had a reflectance of >99.9 % and 15 % at 1.54 and 0.96 μm, respectively. The

output coupler had a reflectance of 80 % at 1.54 μm and 15 % at 0.96 μm. Neither the waveguide length nor the cavity output couplings were optimized.

The Yb-doped waveguide laser was tested using a setup similar to the one shown in Fig 2. The Yb^{3+} device was 10 mm in length. The pump-input mirror had a reflectance of 50 % at 950 nm and 98 % at 1030 nm. Two output couplers with transmittances of 7 % and 21 % at 1020 nm were investigated. These output couplers had reflectances of 32 % and 34 % at 950 nm, respectively.

The configuration shown in Fig 2 was also used to evaluate the slope efficiency and threshold of a Yb/Er-codoped DBR laser. The DBR grating was used as the output coupler instead of the end mounted mirror. To investigate the longitudinal mode structure of the laser we coupled the laser output into an optical fiber scanning Fabry-Perot interferometer with a free spectral range of 124 GHz.

We measured the linewidth of the DBR laser using a conventional self-heterodyne configuration with a 75 MHz frequency shift. [24] The path length difference between the two arms in the self-heterodyne system was 10 km, corresponding to a linewidth resolution limit of 30 kHz for a Gaussian line shape. [25] Optical isolators were used in both arms to prevent optical linewidth narrowing due to feedback; however, the output end of the laser was not beveled.

Several other laser parameters were measured for the DBR laser. We measured the laser wavelengths of other waveguides on the chip using an automatic spectrum analyzer with a resolution of 0.1 nm to determine the variation in wavelength as a function of diffusion aperture width. The excess relative intensity noise (RIN) of the DBR laser formed with an 8 μm diffusion aperture between 0.1 and 1.1 GHz was measured using a

shot noise calibrated RIN measurement system that employs a rf spectrum analyzer. A grating-stabilized, 974-nm pigtailed laser diode served as the pump source. Light from the pump was coupled to a waveguide laser using aspheric lenses. The output power of the DBR laser was set to 2 mW for the measurement. The wavelength of the DBR laser was temperature tuned by varying the temperature of the laser chip from 30 °C to 80 °C using a resistive heater in contact with the waveguide mount.

3. Experimental Results

3.1 Spectroscopic Results and Lifetimes

Figure 3a shows the spectral dependence of absorption and emission cross sections of the erbium ions in Yb/Er-codoped IOG-1. The peak emission cross section of the Er^{3+} using this method was found to be 6.6×10^{-21} cm^2 at 1542 nm. The measured upper state lifetime of the $^4I_{13/2}$ Er manifold was measured to be 8.1 ms in the limit of vanishing excitation power. Figure 3b shows the spectral dependence of the absorption and emission cross sections for IOG-1 glass doped with a Yb concentration of 4×10^{20} cm^{-3}. The peak emission cross section of the $^2F_{5/2}$ laser manifold is 1.27×10^{-20} cm^2 and occurs at a wavelength of 974 nm. The radiative lifetime of the $^2F_{5/2}$ level was measured to be 1.4 ms. The peak absorption cross section was at 974 nm and was 1.28×10^{-20} cm^2. Uncertainties in these reported cross sections are ≤ 20 %. A discussion of the Yb-Er cross relaxation efficiency will follow in the discussion section.

3.2 Waveguide Measurement Results

Visual inspection of the waveguide samples after the ion exchange revealed that regions of the glass surface corresponding to the location of the mask openings had become recessed by approximately 1 μm during the exchange process. The widths of the

recessed channels were close to the widths of the mask apertures and uniform in width and depth. The surface quality of the glass in the recessed regions, observed using a 1000x Nomarski contrast microscope, appears identical to the original surface of the glass and apparently does not cause significant scattering losses. The waveguide end faces were polished perpendicular to the channels. The final sample length was 22 mm.

Figure 4 shows the refractive index depth profile obtained from the refracted ray measurement method at the center of the waveguide formed with the 6.5 μm mask aperture. The data was taken using a wavelength of 635 nm. The spatial resolution is ~1 μm, and the uncertainty of the absolute index value is ~0.001. The index profile indicates a maximum index change of 0.008 that is typical of potassium-sodium ion exchange.

The waveguide supported a single transverse mode having dimensions of 16 μm wide by 11 μm deep (measured at the 1/e points of intensity profile) at 1540 nm. It supported multiple transverse modes at 980 nm. However, when the devices were lasing, the pump energy was confined primarily within the lowest order transverse mode, which had dimensions of 13 μm wide by 9.5 μm deep. The uncertainty of the mode dimensions determined using this method are ~10 %.

3.3 Yb/Er Fabry-Perot Waveguide Laser Measurement Results

The laser output power as a function of coupled pump power for the 22 mm device pumped at 960 nm, is shown in Figure 5. We estimated the coupling efficiency of the incident pump power to be between 65 and 71 %, including losses due to the transmittance of the input mirror and launching objective. The coupled pump power shown on the x-axis in Figure 5 was calculated based on a 71 % coupling efficiency. The uncertainty of the power measurements are estimated to be 5 %. The threshold pump power was 23

mW, and the slope efficiency was 28 %. One end of the waveguide was accidentally chipped during our experiments and necessitated the repolishing of the end face. The output powers as a function of coupled pump powers of the resulting 20-mm long waveguide laser, when pumped at 979 nm, are also shown in Fig. 5. The launched pump power threshold was 51 mW, and a maximum output power of 170 mW was obtained for 610 mW of launched pump power. At these power levels, there was no change in the slope efficiency as a function of pump power, suggesting that the Yb ions are not saturating as they do in Yb/Er-codoped silica fiber lasers. [26]

The Yb/Er-laser usually operated at several wavelengths simultaneously. A typical laser spectrum showing simultaneous operation at 1.536, 1.541, and 1.545 μm is depicted in Figure 6. The laser spectrum could be shifted in wavelength by passing some of the collimated 1.5 μm laser output through a prism and reflecting it back through the prism and into the waveguide using a dielectric mirror. This operation formed a weakly coupled, external cavity. The cavity is shown in Fig. 7a. Rotating the output coupler mirror produced wavelengths ranging from 1536 to 1595 nm.

Tuning of the laser was also accomplished using the extended cavity configuration shown in Figure 7b. We used a first order grating with a reflectance of 0.6 for the laser output coupler. We rotated the grating and could tune the laser from 1525 nm to 1564 nm when the coupled pump power was 280 mW at a wavelength of 980 nm. The laser output power as a function of wavelength is illustrated in Fig. 8a. Three representative spectra of the laser are shown in Fig. 8b.

3.4 Yb-doped waveguide laser measurement results

The laser output power as a function of launched pump power is shown in Figure 9. The launching efficiency of the pump for these measurements was 45 %. For the 7 % output coupler, the threshold when pumped at 949 nm was 18 mW of coupled pump power. For the 21 % output coupler, the threshold pump power was 25 mW, and up to 120 mW of output power was obtained. The slope efficiency was 67 % when based on coupled pump power.

Like the Yb/Er laser, the Yb laser typically operated at several wavelengths simultaneously. At lower pump powers, the longer wavelength transitions dominate due to ground state re-absorption losses, which are larger at shorter wavelengths. As the pumping intensity in the waveguide increases, the Yb-ion ground state population and hence the ground state re-absorption loss is reduced, and the shorter wavelength transitions, which lie closer to the peak of the Yb^{3+} emission cross section, are favored.

The Yb-doped waveguide laser was tuned by reflecting some of the collimated laser output power back into the waveguide using the first-order reflection from a diffraction grating having 1200 grooves/mm. The cavity was similar to Fig. 7b. Rotating the grating tuned the laser continuously from 986 nm to 1050 nm.

3.4 Single-frequency Yb/Er-codoped DBR lasers

Figure 10 shows the DBR laser output power as a function of launched pump power and the spectrum of the laser. The waveguide diffusion aperture for this waveguide was 8 μm. The slope efficiency as a function of launched pump power is calculated to be 26 % when we take the pump coupling factor to be 71 %.

We estimated the reflectance of the grating using the simplified laser formula derived from the theory of Rigrod:[27]

$$\frac{P_1}{P_2} = \frac{1 - R_1}{1 - R_2}\sqrt{\frac{R_2}{R_1}} \qquad (2),$$

where P_1 is the output power at the grating end and P_2 is the output power at the end opposite the grating. R_1 is the grating reflectance and R_2 is the reflectance of the attached mirror. We used two mirrors with reflectances of 80 and 90 percent for R_2. For both cases we calculated the grating reflectance R_1 to be 65 percent.

Figure 11 shows that the laser operated on a single longitudinal mode when the coupled pump power did not exceed 300 mW. The laser was robustly single frequency with TE polarization, and no mode hopping was observed. The inset in Figure 11 shows that a second longitudinal mode appeared when the coupled pump power exceeded 300 mW. In this pump regime, the laser was unstable and exhibited mode hopping, single-frequency operation, and dual-frequency operation. By measuring the frequency spacing between the longitudinal modes we determined that the effective physical length of the laser cavity was 1.4 cm.

Figure 12 shows the self-heterodyne spectrum. The laser linewidth we obtained from this measurement was 500 kHz. Seven of the eleven waveguides on the chip exhibited laser oscillation. The waveguides formed through the smaller apertures did not achieve threshold because the smaller mode volumes caused a reduction of the gain such that the 35 % transmittance loss of the grating could not be overcome. Table 3 shows the laser operating wavelengths as we scanned the comb of waveguides that had diffusion aperture widths ranging from 5 to 8 μm. In general, the wavelength increases as the diffusion aperture width increases, which is consistent with increasing effective index as the

aperture width increases. A visible defect was apparent on waveguide No. 4 that caused a deviation from the trend.

The results of the RIN measurements are shown in Figure 13. Figure 13a shows that the RIN dropped to less than -150 dB/Hz for frequencies above ~0.5 GHz. The data have not been smoothed. We estimate the uncertainty in the RIN to be 2 dB/Hz. By measuring the relative amplitude noise (with respect to the noise floor) between 100 kHz and 10 MHz, we found that the relaxation oscillation peak was located near 350 kHz as shown in Fig. 13b. These noise measurements are consistent with those of Er-doped fiber lasers, and we expect lower RIN when the laser is operated further above threshold.[26]

The wavelength as a function of temperature is shown in Fig. 14. The tuning range for the test laser varied linearly from 1536 nm to 1536.8 nm for a change in wavelength $\Delta\lambda$, of 0.8 nm. This tuning range matches well with the predicted tunability of the laser of 0.6 nm over 50 °C. The prediction is based on the thermal expansion coefficient of the glass and the change in refractive index as a function of the change in temperature, and is approximated by the following equations:

$$\Delta\lambda \cong 2\Lambda\frac{\Delta n}{\Delta T}\Delta T + 2n\Lambda\left(\frac{1}{\Lambda}\frac{\Delta\Lambda}{\Delta T}\right)\Delta T; \quad \frac{\Delta n}{\Delta T} = -3.2\times10^{-6}/^{\circ}C; \quad \frac{1}{\Lambda}\frac{\Delta\Lambda}{\Delta T} = 1\times10^{-5}/^{\circ}C \quad (3)$$

where Λ is the grating period and n is the refractive index of the glass. The wavelength stability as a function of temperature is roughly 15 times smaller than that of typical semiconductor DFB lasers.[28] Thus the temperature control requirements for maintaining a stable wavelength are relaxed.

4. Discussion

It is important to note that the lengths of 22 mm and 20 mm are not optimum lengths for these Yb/Er-codoped waveguide lasers. Using a waveguide laser simulation tool, we predicted the laser output characteristics as a function of length and waveguide mode-field size. The simulation is based on a phenomenological model which incorporates the Yb/Er laser rate equations on a three dimensional grid, the forward and backward propagating laser signals, and the forward propagating pump signal.[29] The propagating intensity profiles were approximated by elliptical functions that approximated the measured transverse laser mode dimensions and the fundamental pump mode dimension. The glass and laser parameters we used in the model are listed in Table 2. The Yb-Er cross relaxation coefficient (C_{cr}) and the cooperative upconversion coefficient (C_{up}) were the fitting parameters. Reasonable approximations of other laser and waveguide parameters based on actual measurements and analyses were used for other quantities. Figure 5 shows the actual laser data compared to results of the laser simulation. We used C_{cr}= 3.5×10^{-16} cm^3/s and $C_{up} = 2.5 \times 10^{-18}$ cm^3/s to obtain the best fit. Using C_{cr} and the approximate equation for cross relaxation quantum efficiency,

$$\eta = \frac{C_{cr} N_{Er} \tau_{21}^{Yb}}{1 + C_{cr} N_{Er} \tau_{21}^{Yb} (1 + \tau_{32}^{Er} N_{Yb} / \tau_{21}^{Yb} N_{Er})} \qquad (1)$$

from reference 6, we calculated the cross relaxation quantum efficiency to be 97 %, a typical efficiency for phosphate glasses.[17] In this equation, we assumed that the lifetime, τ_{32}, is approximately 2.8 μs.

Simulations using different waveguide laser lengths ranging from 1 to 2 cm were performed. Figure 15 shows how the output power varies as a function of cavity length for several output coupling reflectances ranging from 80 to 95 %. and constant laser pump power of 500 mW. Figure 16 shows the output power as a function of mode width, mode depth and output mirror reflectivity for optimized waveguide lasers. The best solutions are color-coded in red; these ranged from 175 to 185 mW continuous wave output, assuming a nominal cavity length of 1 cm and launched 974-nm pump power of 500 mW. The optimum solution has an output mirror reflectance of 82.9%, a laser mode field with dimensions 6 μm by 12 μm, and a continuous-wave output power of 184 mW at 1.54 μm. The optimization used an adaptive simulated anncaling algorithm[30] , driven by a waveguide solver [31] and the laser rate equation model[29]. Details of the optimization method will be presented in a later paper.

5. Conclusions

In summary, we have presented an introduction to the development of phosphate-based laser glass for the fabrication of waveguide lasers. Recent results obtained for Yb/Er-codoped waveguide lasers formed by ion exchange in IOG-1 base glass show a dramatic improvement over previously demonstrated waveguide lasers. The lasers presented in this paper have produced output powers in the 1500 nm telecommunication window approaching 200 mW without saturation. Slope efficiencies of 28 % have been achieved. Wavelength tuning has been performed over 70 nm using external cavities. Simulations of Yb/Er-doped waveguide lasers indicated that further improvement of laser performance is possible by optimizing output coupling, cavity length, and doping concentrations. Low-noise DBR lasers that operate on a single longitudinal mode at 1536

nm have been fabricated and tested. The fabrication process can be applied to the manufacture of monolithic laser arrays with wavelengths conforming to the ITU grid for wavelength-division-multiplexed telecommunications. In addition to these results, we have demonstrated Yb-doped waveguide lasers in phosphate glass operating over a wavelength range of 986 to 1050 nm. These demonstrations of efficient integrated optical lasers clearly show that waveguide lasers are a promising new technology that can be used in many applications that have previously been the domain of semiconductor laser sources.

Acknowledgement

The authors acknowledge the National Science Foundation (PHY-94-15583) and the U.S. Army Research Office (DAAH04-95-1-0300) for support of the University of Rochester effort.

Table 1: IOG-1 Base Glass Composition (mole %)

P_2O_5	60
Na_2O	24
Al_2O_3	13
R_2O_3	3
R = Σ Rare Earths	

Table 1. Veasey

Table 2. Parameters used to model the Yb/Er codoped waveguide laser

Length of Waveguide Laser Cavity	L = 2 cm
Signal Field diameters (elliptical 1/*e* full width)	W_{sx}= 16 μm, W_{sy} = 11 μm
Pump Field diameters (elliptical, 1/*e* full width)	W_{px}=13 μm, W_{sy} = 9.5 μm
Signal Effective Index	n_s = 1.515
Pump Effective Index	n_p = 1.515
Spontaneous Emission Lifetime of $^4I_{13/2}$	τ_{21} = 8.1 ms = $1/A_{21}$
Stimulated Emission Cross Section @ 1540 nm ($^4I_{13/2}$-$^4I_{15/2}$)	$\sigma_{21} = 4.62 \times 10^{-21}$ cm^2
Absorption Cross Section @1540 nm ($^4I_{15/2}$-$^4I_{13/2}$)	$\sigma_{12} = 4.13 \times 10^{-21}$ cm^2
Er Pump Absorption Cross Section @ 977 nm ($^4I_{15/2}$-$^4I_{11/2}$)	$\sigma_{13} = 1.9 \times 10^{-21}$ cm^2
Yb Absorption Cross Section @ 977 nm ($^2F_{7/2}$-$^2F_{5/2}$)	$\sigma_{56} = 1.04 \times 10^{-20}$ cm^2
Yb Emission Cross Section @ 977 nm ($^2F_{5/2}$-$^2F_{7/2}$)	$\sigma_{65} = 1.19 \times 10^{-20}$ cm^2
Yb-Er Cross Coupling Coefficient C_{er}	Fitting parameter, see text
Upconversion Coefficient C_{up}	Fitting parameter, see text
Signal Wavelength	λ_s = 1540 nm
Pump Wavelength	λ_p = 977 nm
Er Ion Density	$N_{er} = 1 \times 10^{20}$ cm^{-3}
Yb Ion Density	$N_{yb} = 4 \times 10^{20}$ cm^{-3}
High Reflector Reflectance	R_1 = 0.9995
Output Coupler Reflectance	R_2 = 0.80
Nonradiative Lifetime of Level $^4I_{11/2}$	τ_{32} = 2.8 μs ≈ $1/A_{32}$
Excess Waveguide Scattering Loss	α_{is} = 0.1 dB/cm α_{ip} = 0.2 dB/cm

Table 2. Veascy

Table: 3. :List of waveguides, mask aperture widths, and corrcsponding DBR laser output wavelengths

Waveguide	Aperture width (μm)	Wavelength (nm)
1	8.0	1536.02
2	7.5	1536.09
3	7.0	1536.05
4*	6.5	1535.15
5	6.0	1536.26
6	5.5	1536.24
7	5.0	1536.32

* observed defect in sample

Table 3. Veasey

Figure 1. Veasey

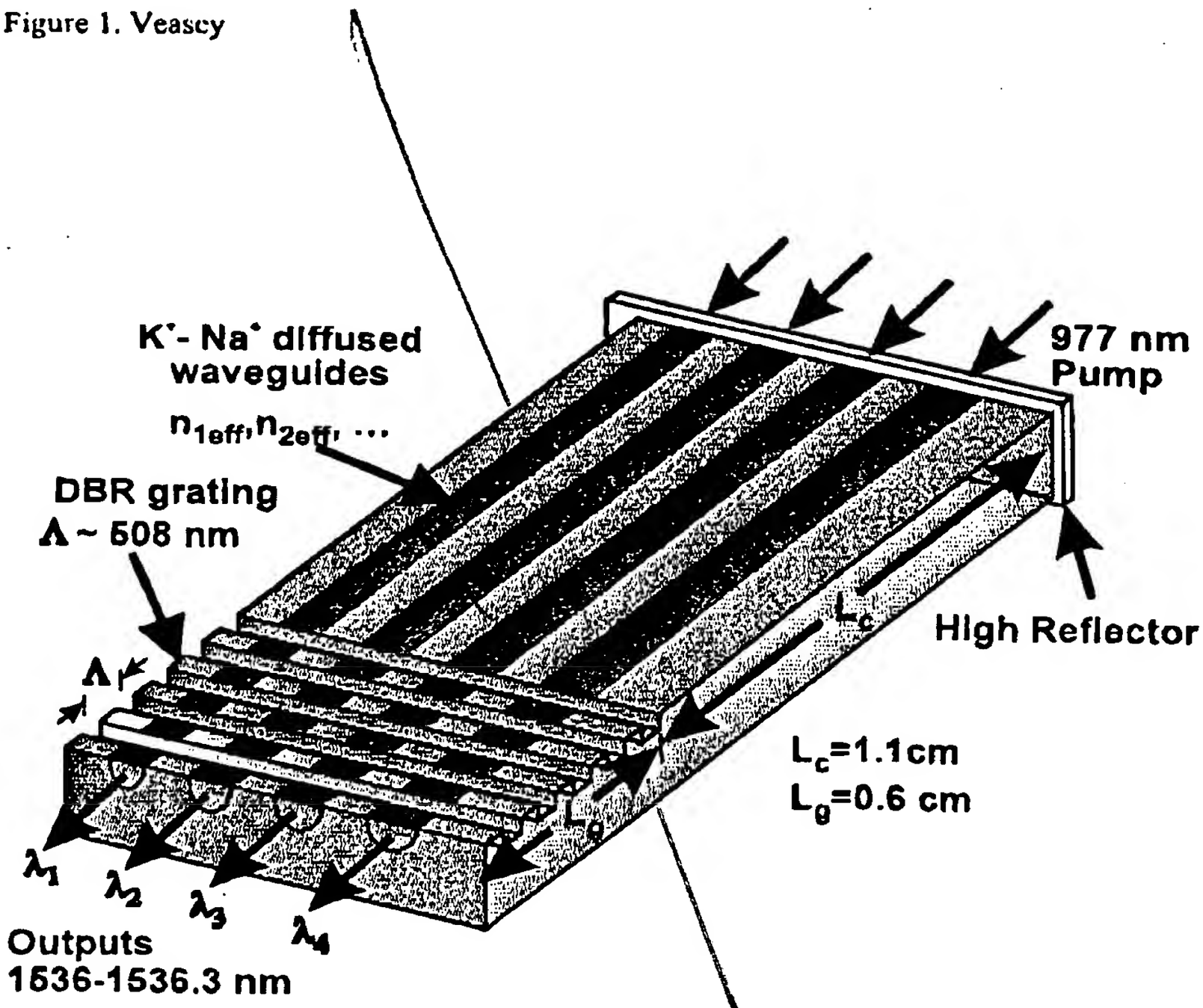

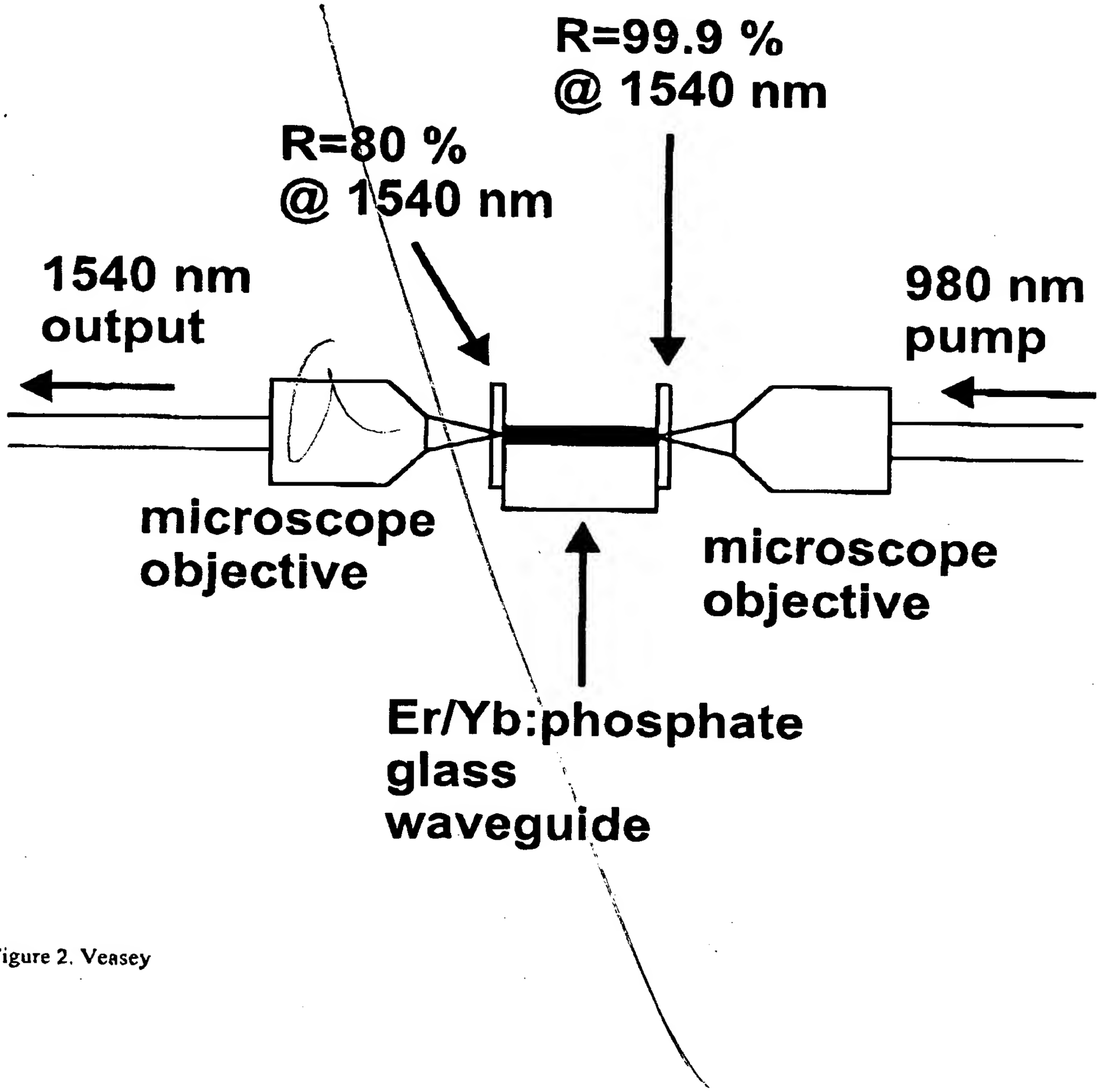

Figure 2. Veasey

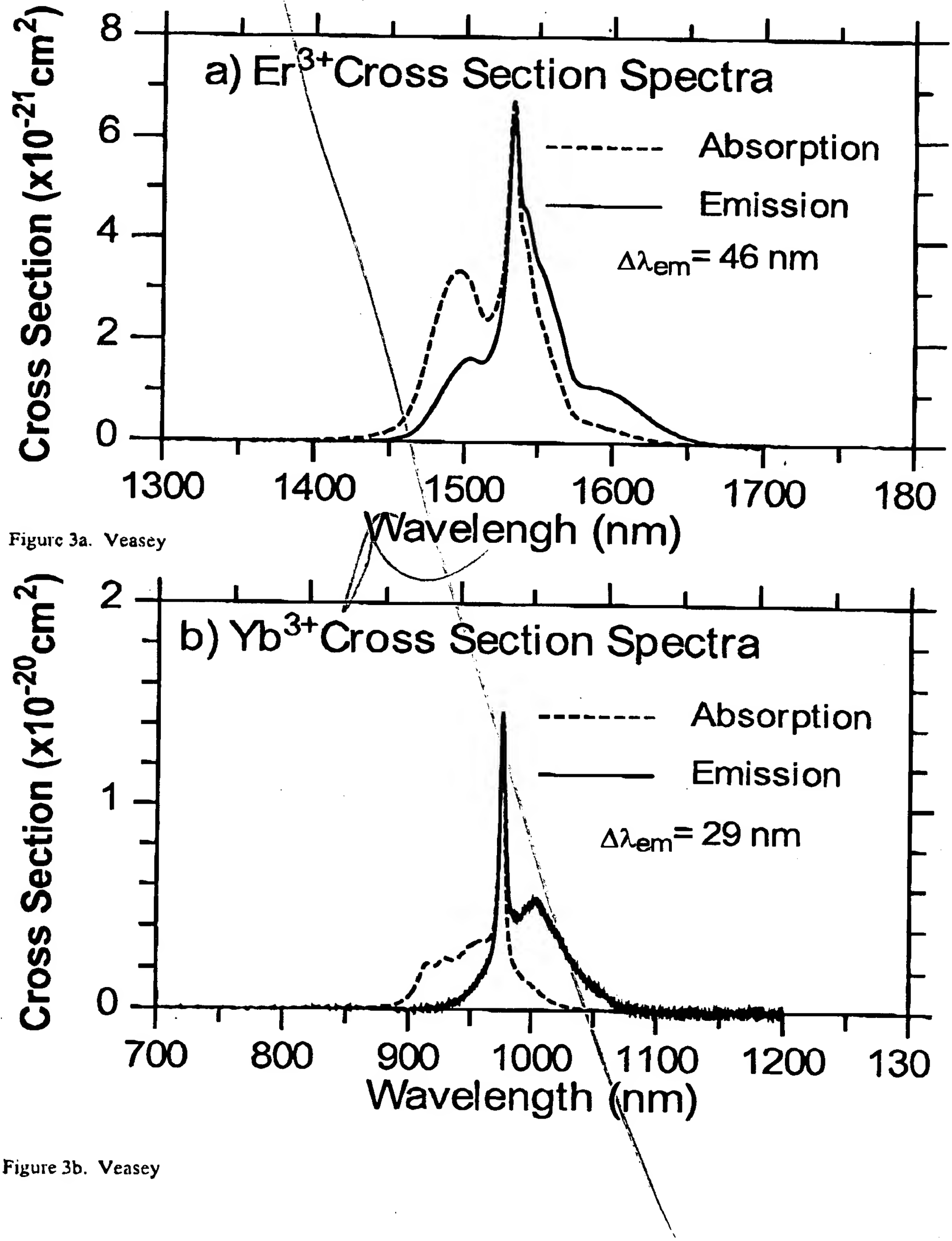

Figure 3a. Veasey

Figure 3b. Veasey

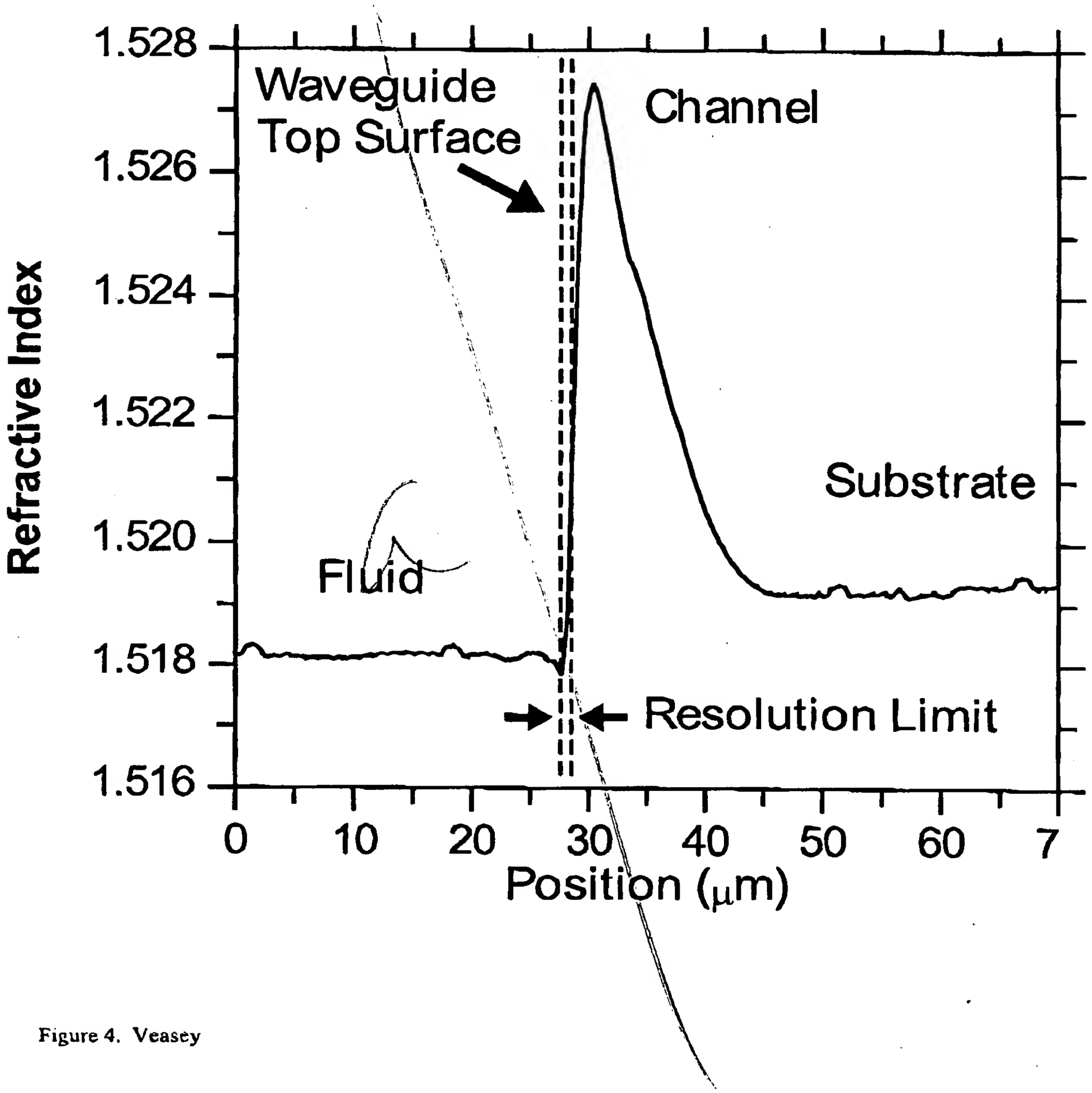

Figure 4. Veasey

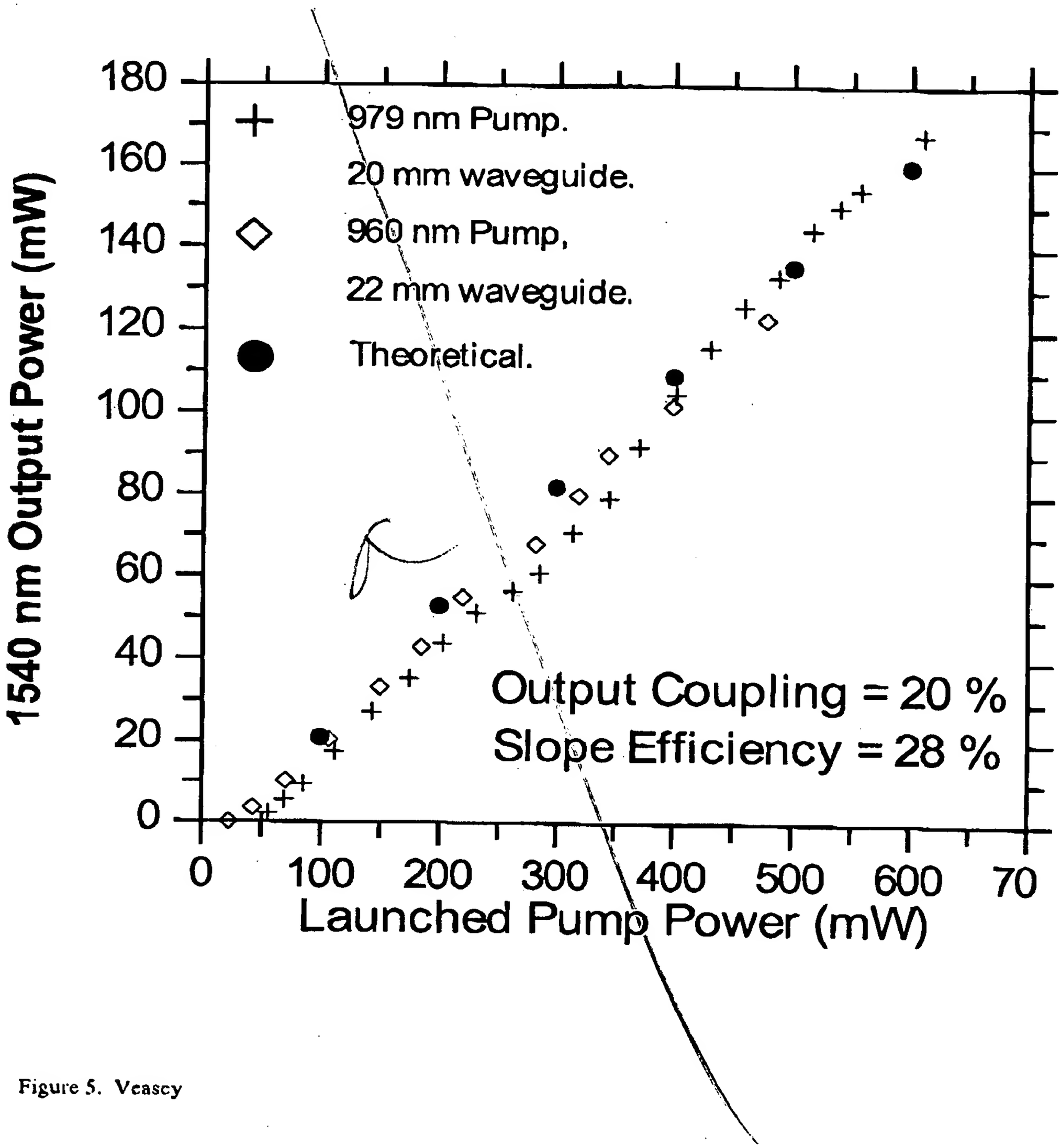

Figure 5. Veascy

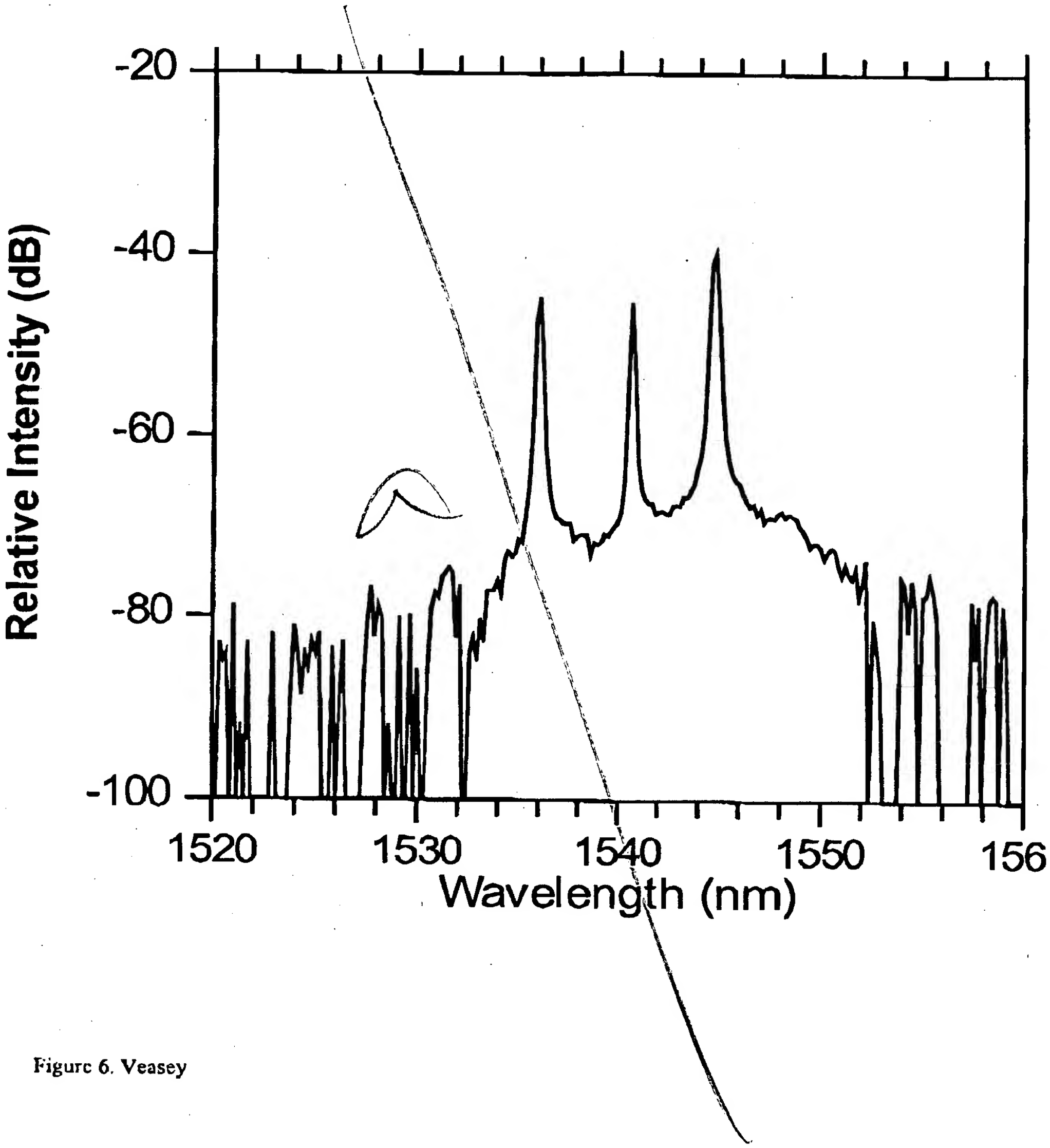

Figure 6. Veasey

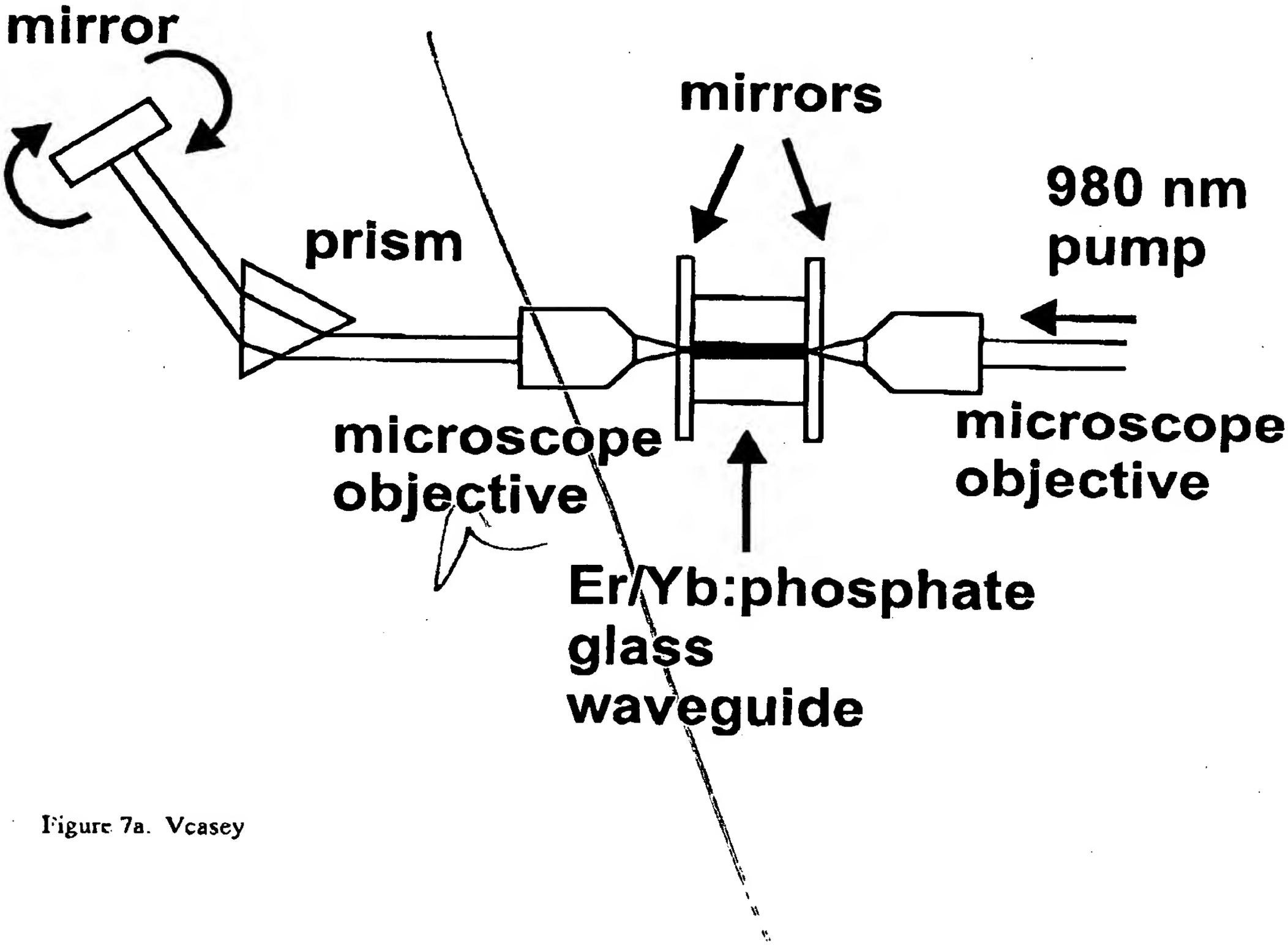

Figure 7a. Vcasey

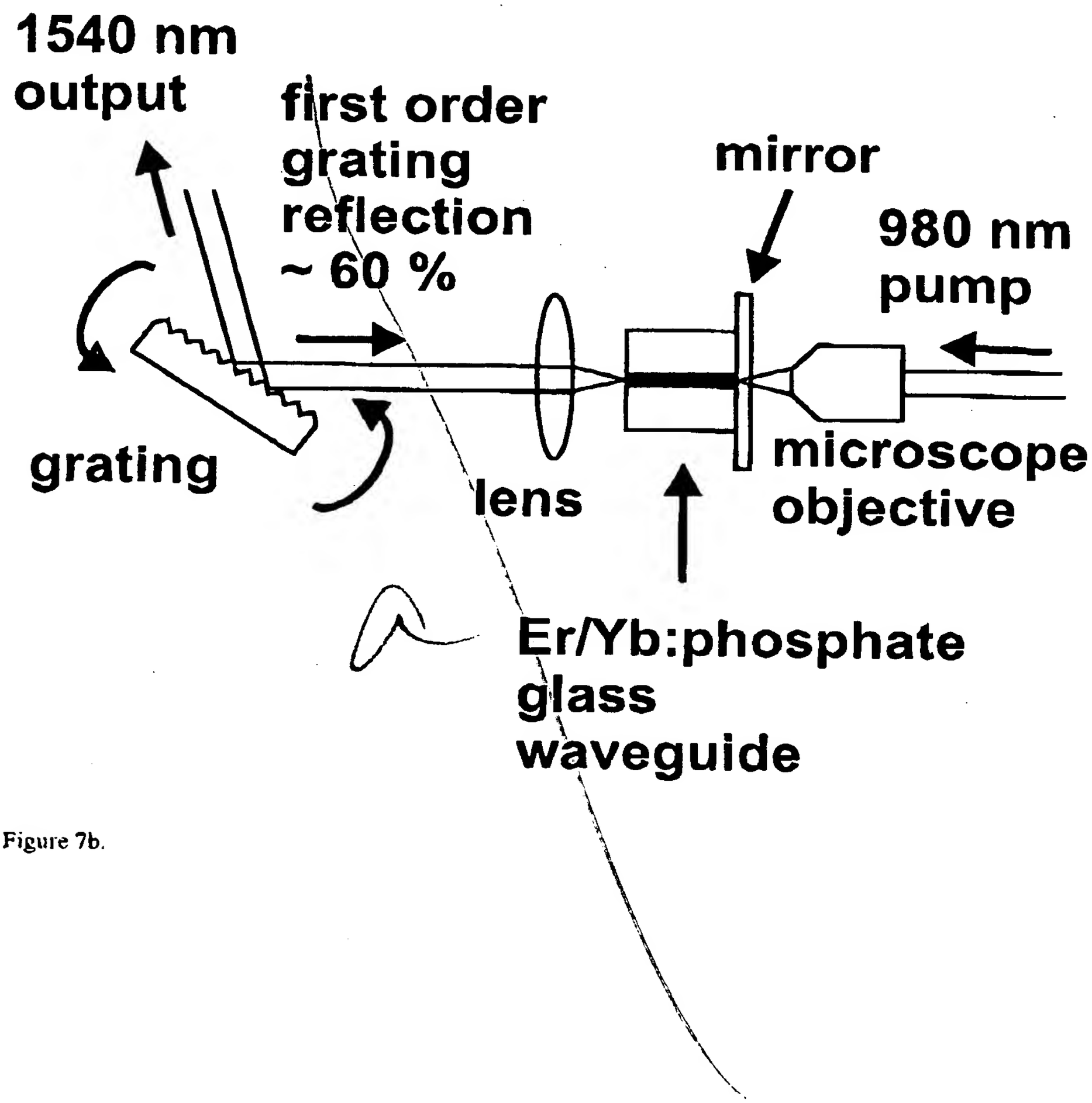

Figure 7b.

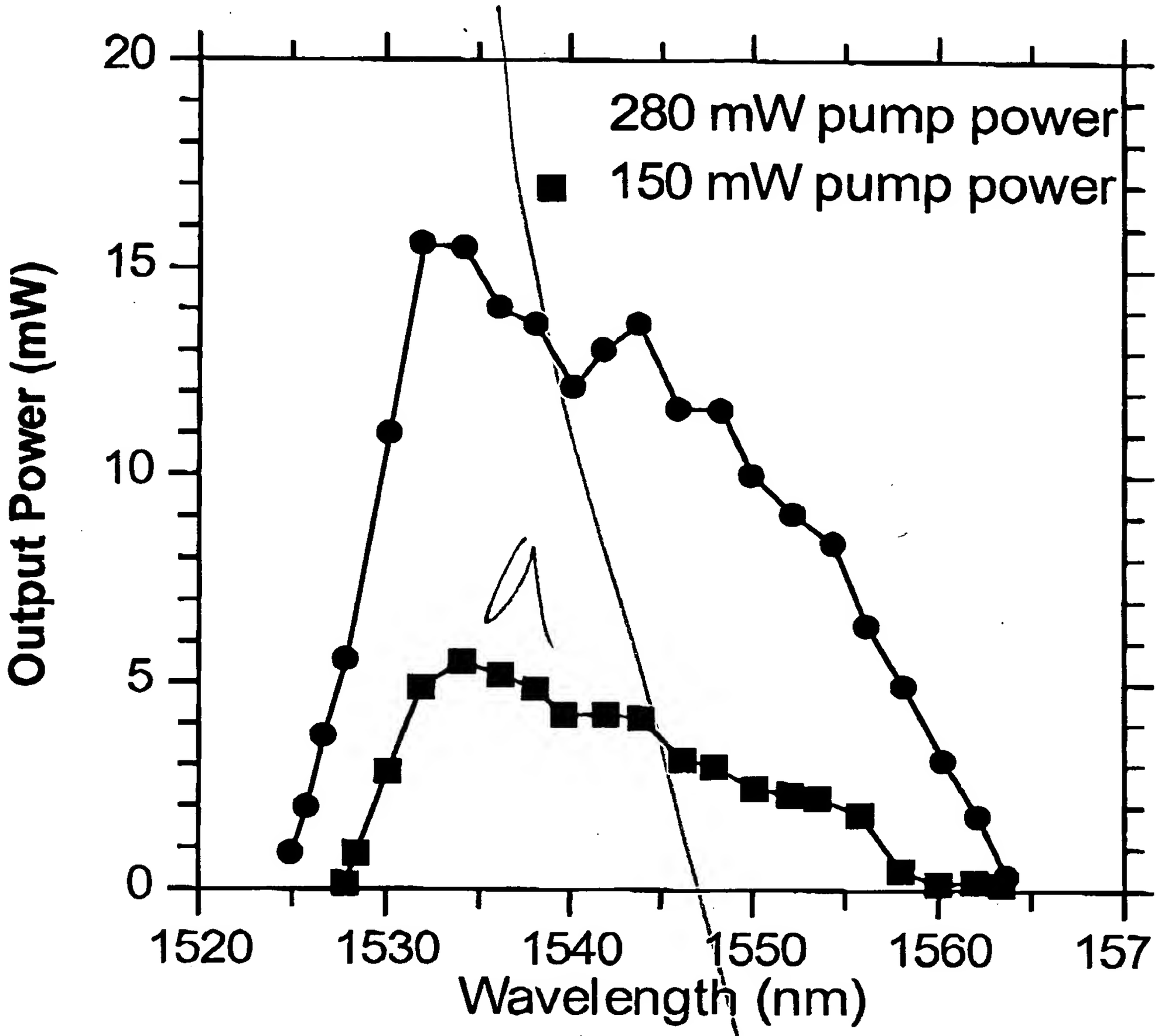

Figure 8a. Vcasey

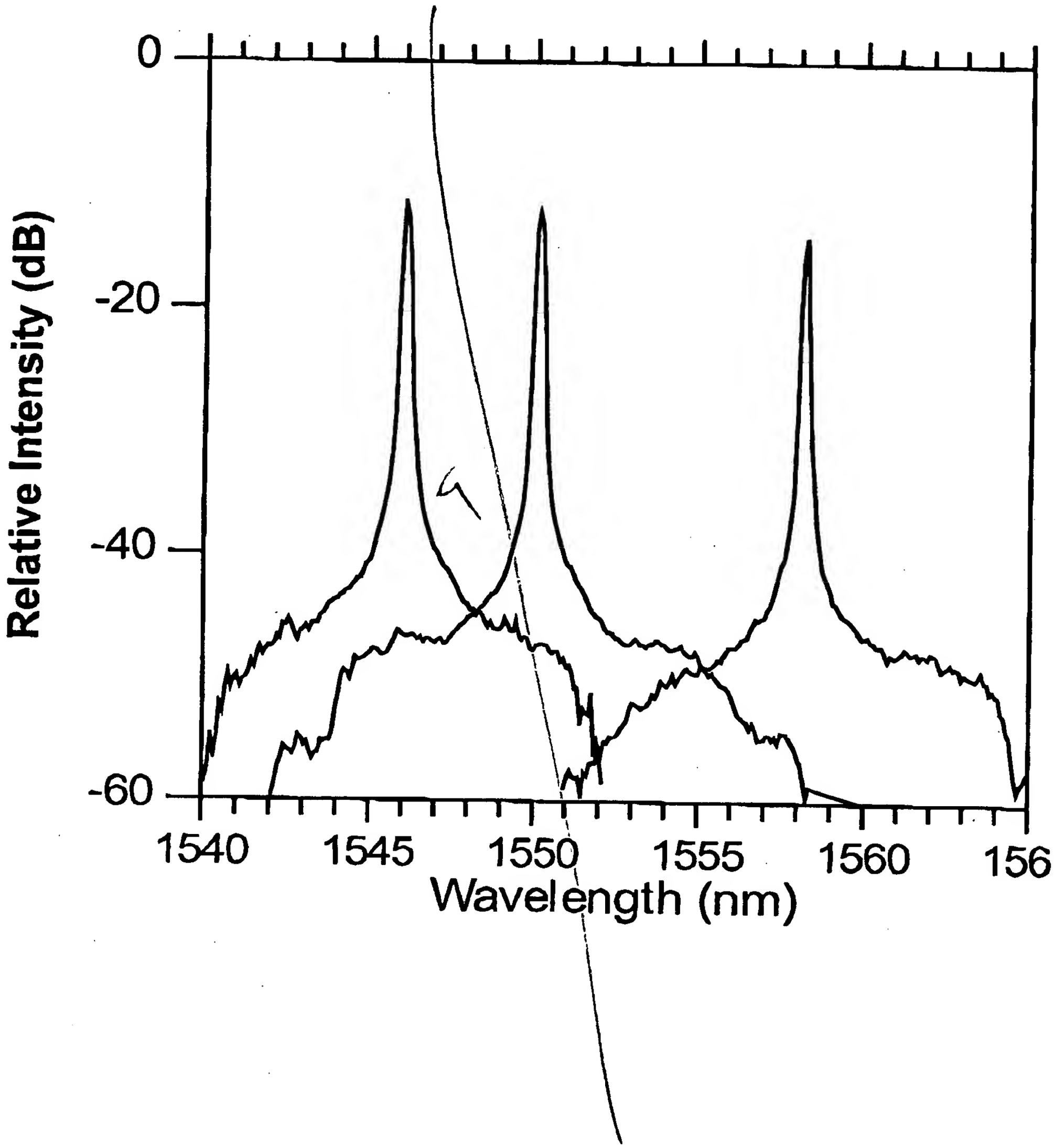

Figure 8b. Veasey

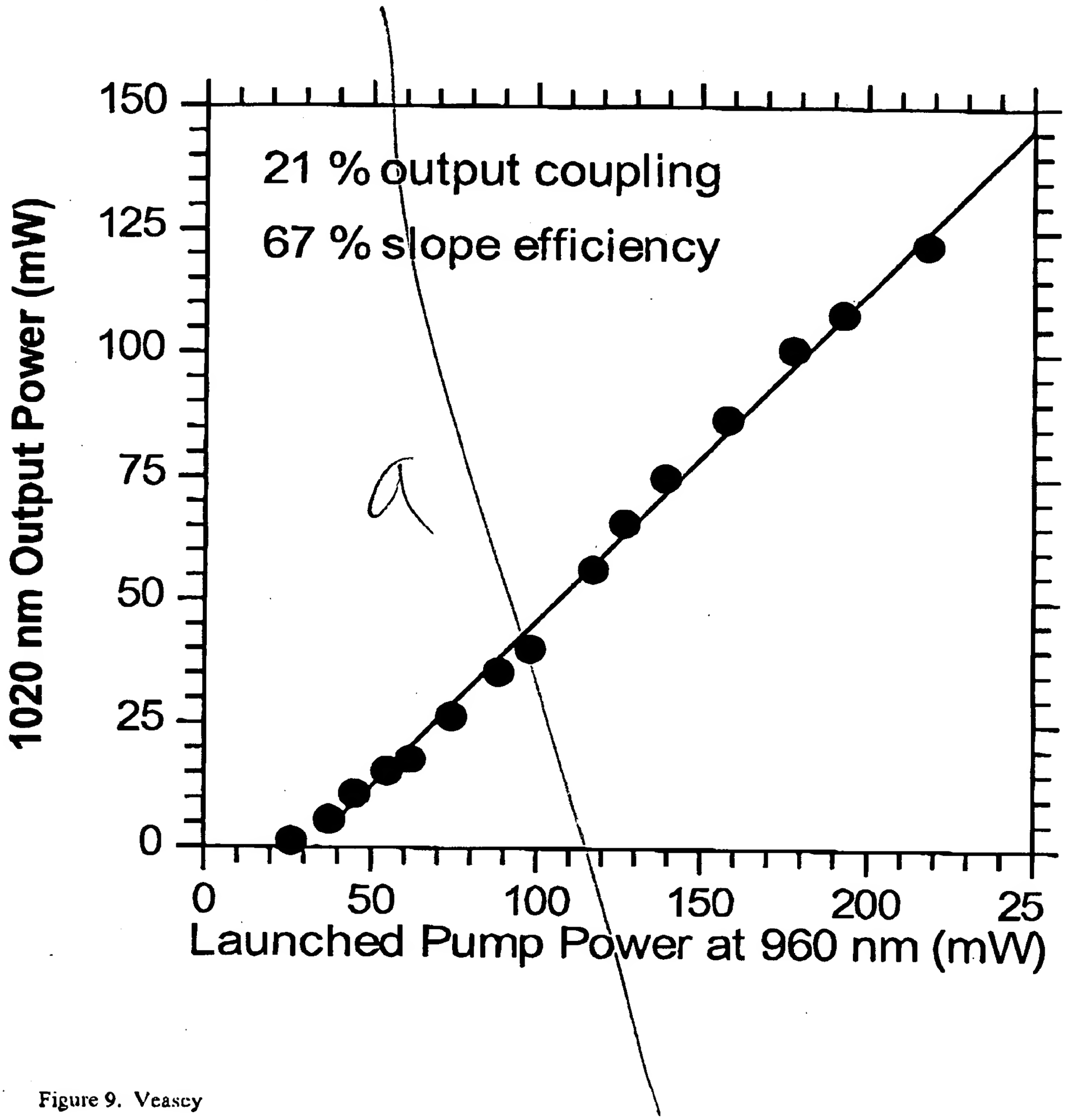

Figure 9. Veascy

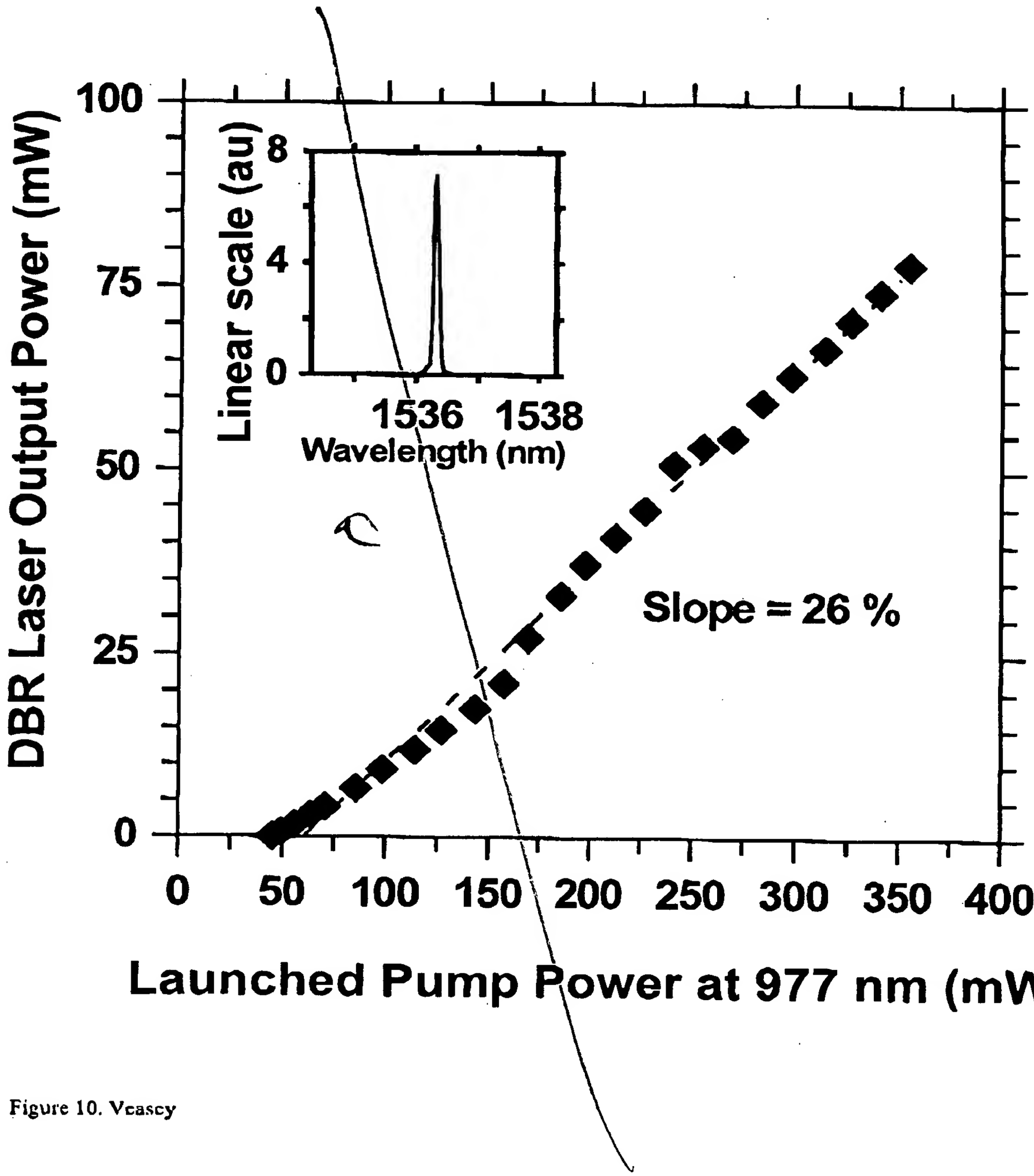

Figure 10. Veascy

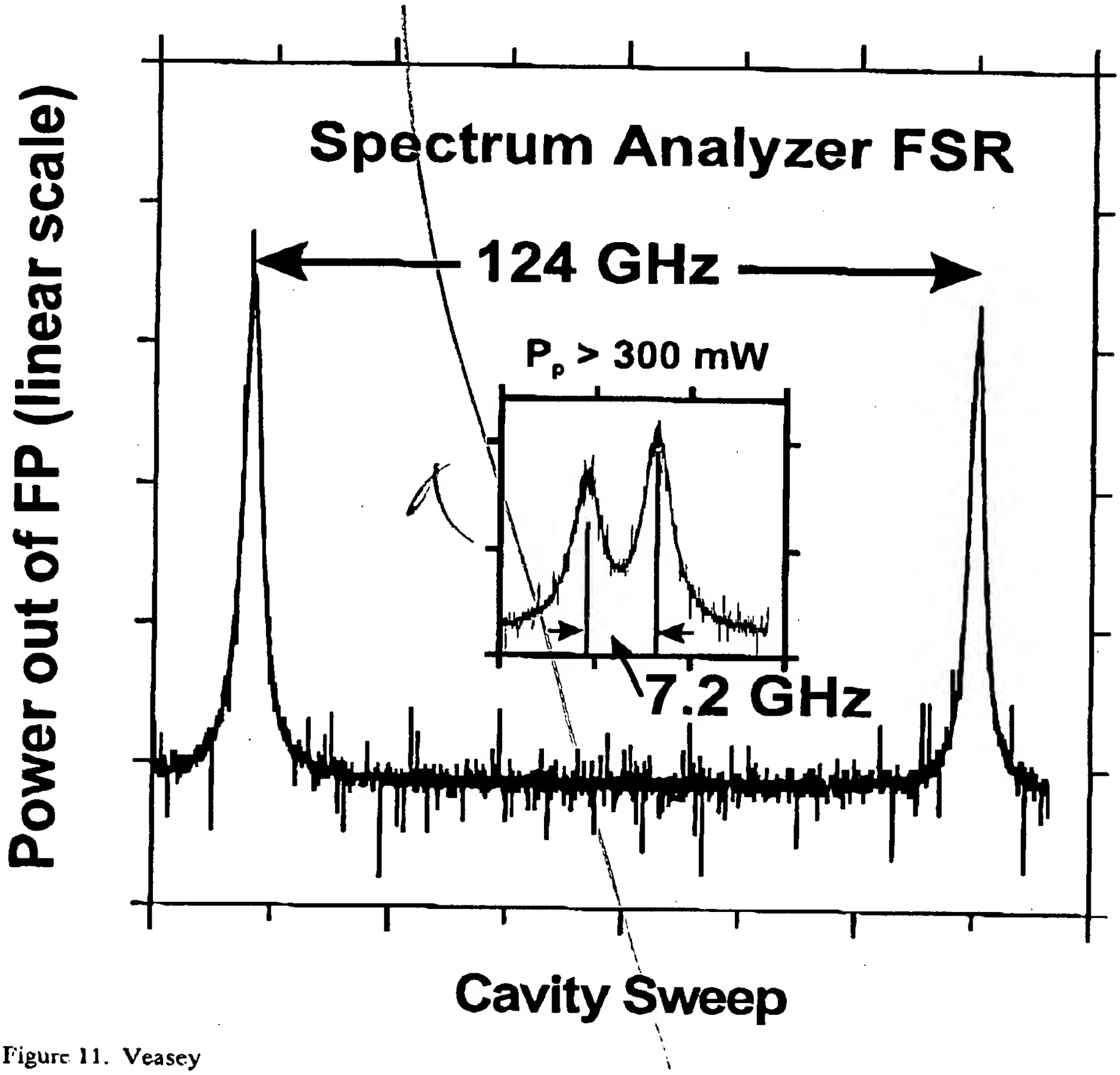

Figure 11. Veasey

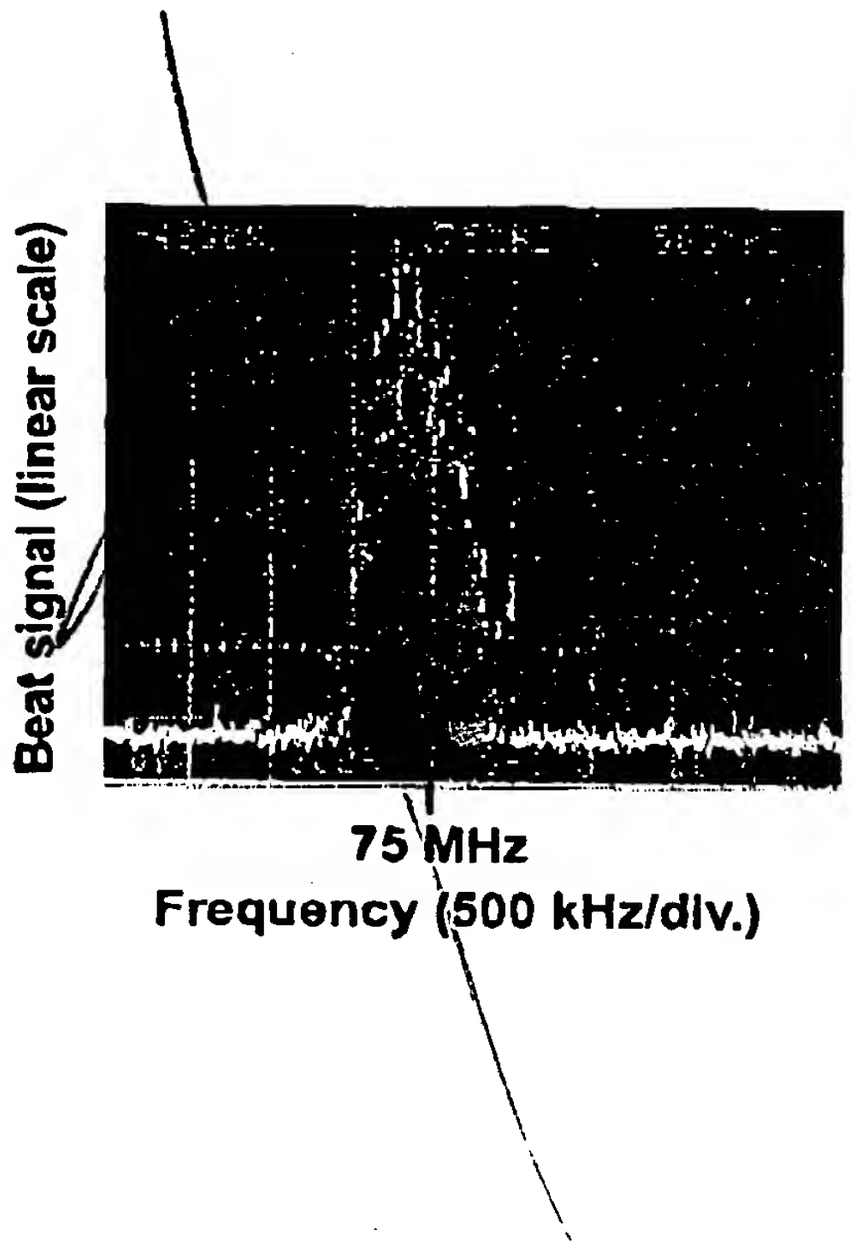

Figure 12. Veascy

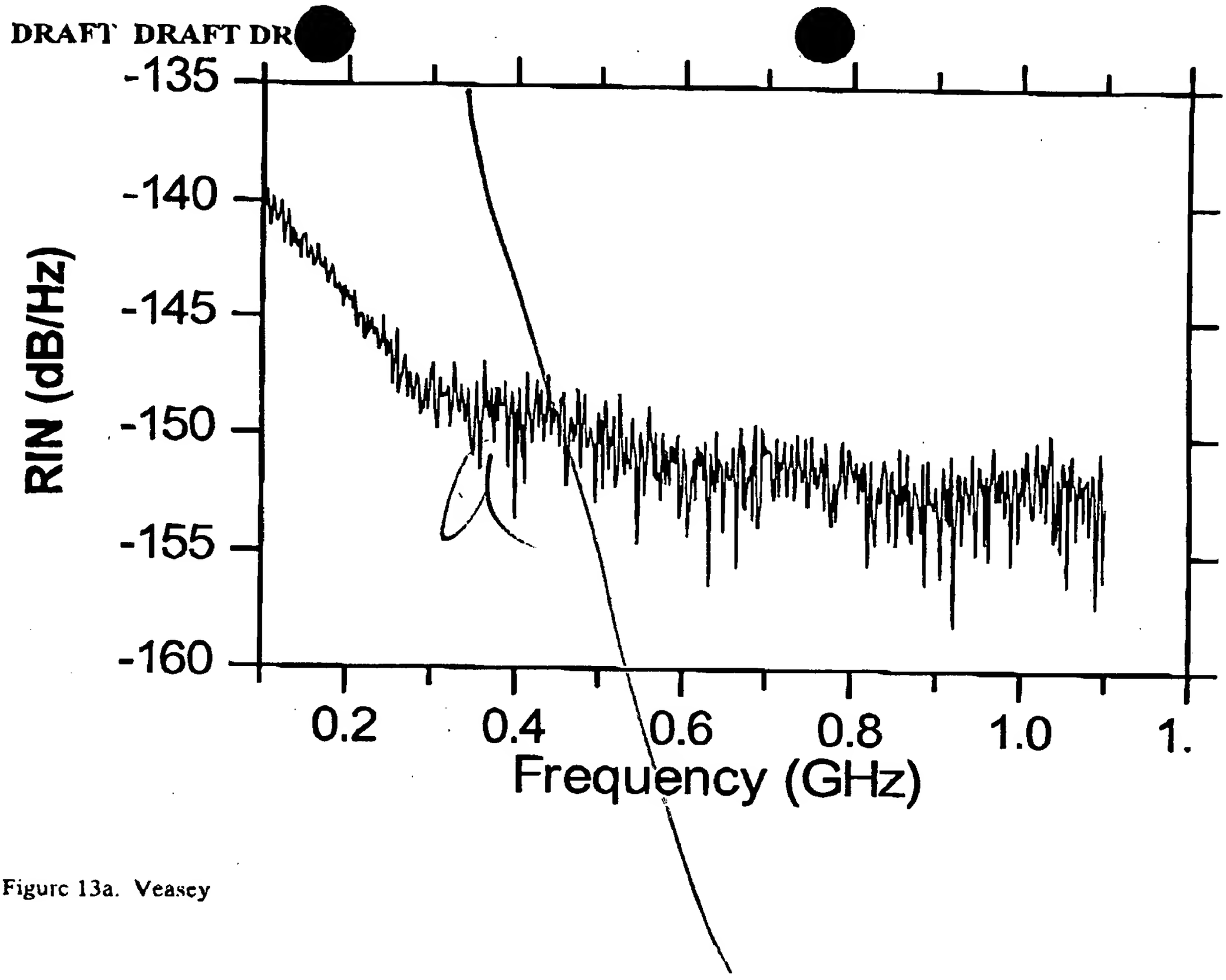

Figure 13a. Veasey

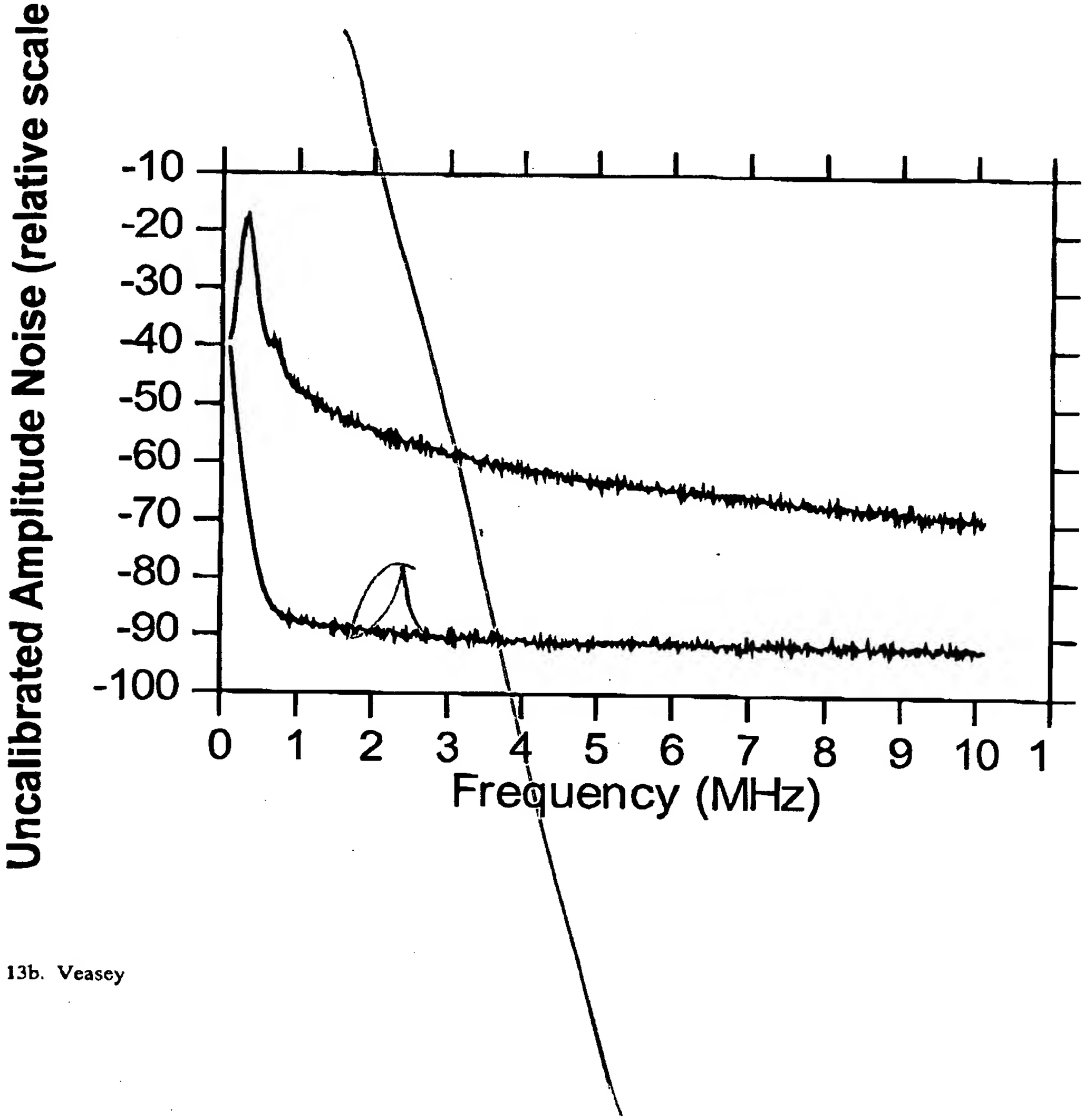

Figure 13b. Veasey

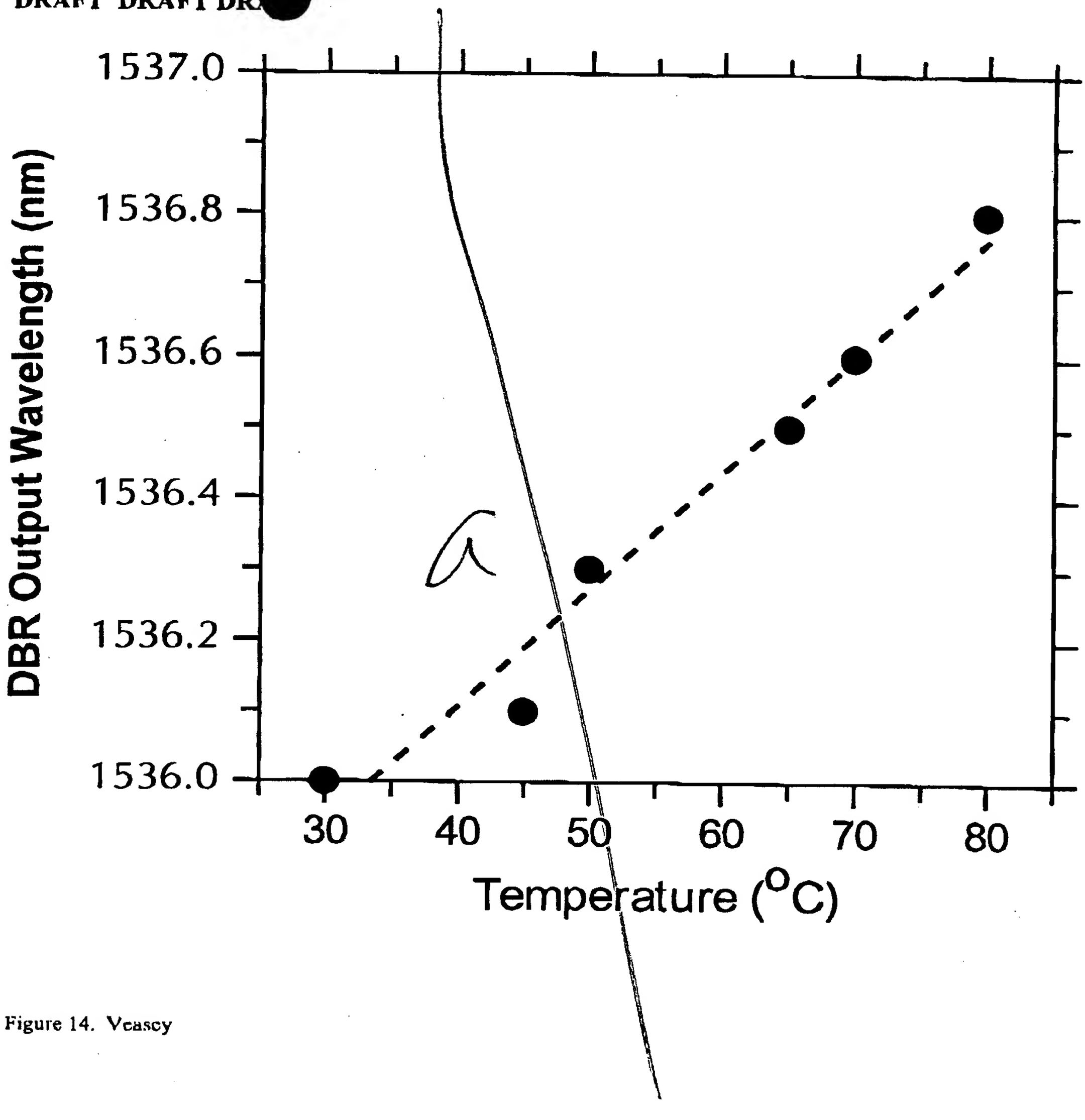

Figure 14. Veascy

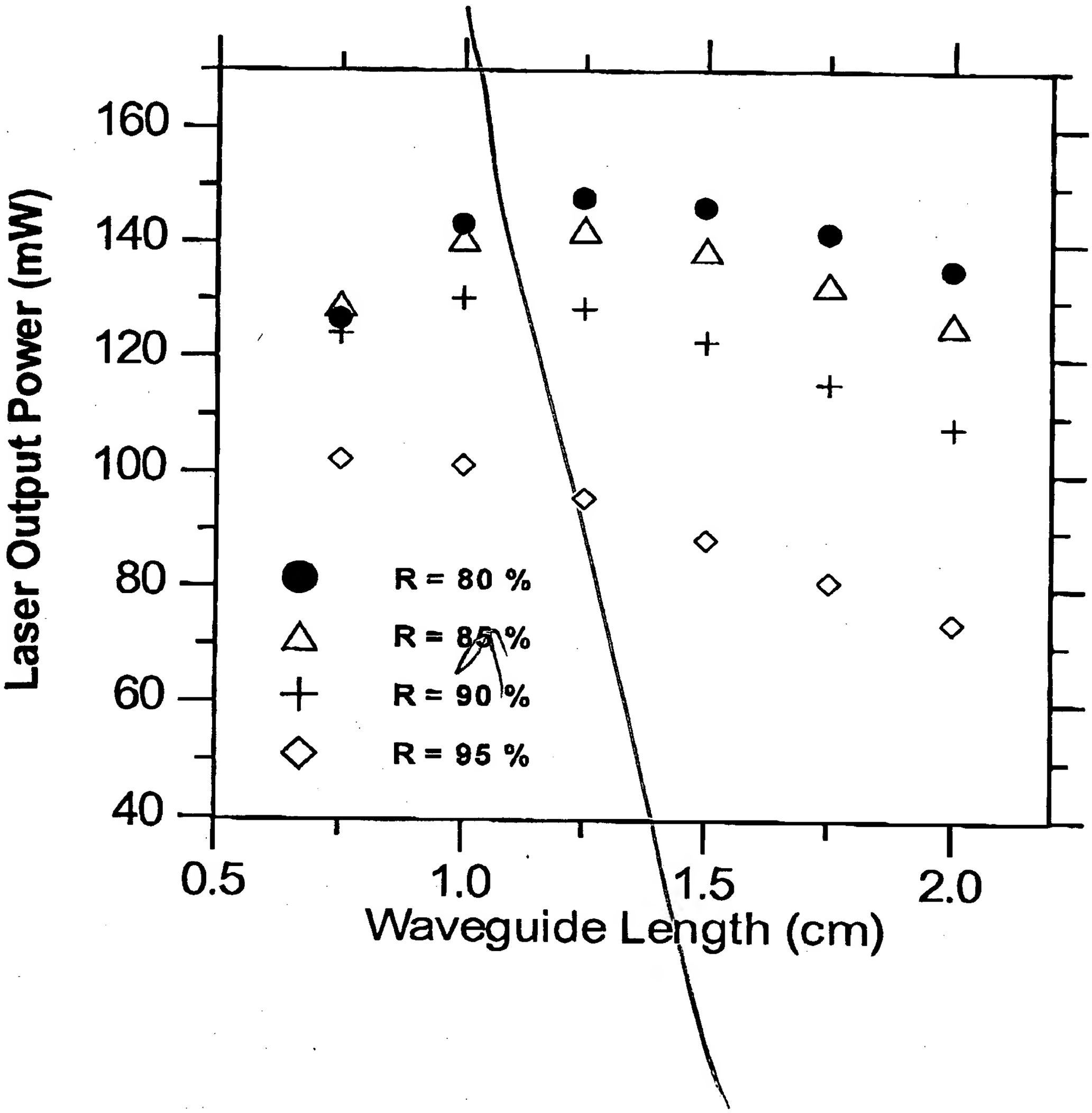

References

[1] M. Saruwatari and T. Izawa, Appl. Phys. Lett. 24, 603 (1974).

[2] K.J. Malone, N.A. Sanford, and J.S. Hayden, Electron. Lett. 29, 691 (1993).

[3] T. Feuchter, E.K. Mwarania, J. Wang, L. Reekie, J.S. Wilkinson, IEEE Photon. Technol. Lett. 4, 542, (1992).

[4] D. Barbier, J. Hubner, J.M. Jouanno, A. Kevorkian, A. Lupascu, Post deadline Conf. Digest, European Conf. On Integrated Optics (1993).

[5] G.L. Vossler, C.J. Brooks, and K.A. Winik, Electron. Lett. 31, 1162 (1995).

[6] J.E. Roman, M. Hempstead, W.S. Brocklesby, S. Nouh, and J.S. Wilkinson, P. Camy, C. Lerminiaux, and A. Beguin, Post deadline Conf. Digest, European Conf. On Integrated Optics, (1995).

[7] P. Fournier, P. Meshkinfam, M.A. Fardad, M.P. Andrews, and S.I. Najafi, Electron. Lett. 33, 293 (1997).

[8] F.D. Patel, E.C. Honea, D. Krol, S.A. Payne, J.S. Hayden, Conf. Digest, OSA Advanced Solid State Laser Conference, p. 338, (1999).

[9] J. Shmulovich, A. Wong, Y.H. Wong, P.C. Becker, A.J. Bruce, and R. Adar, Electron. Lett 28, 1181 (1992).

[10] Y.C. Yan, A.J. Faber, H. de Waal, P.G. Kik, and A. Polman, Appl. Phys. Lett 71, 2922 (1997).

[11] S. Guldberg-Kjaer, J. Hubner, M. Kristensen, C. Laurent-Lund, M. Rysholt Poulsen, and M.W. Sckerl, Electron. Lett. 35, 302, (1999).

[12] T. Kitagawa, K. Hattori, M. Shimizu, Y. Ohmori, M. Kobayashi, Electron. Lett. 27, 334 (1991).

[13] G.N. van den Hoven, R.J.I.M. Koper, A. Polman, C. van Dam, J.W.M. van Uffelen, and M.K. Smit, Appl. Phys. Lett. 68, 1886 (1996).

[14] R. Serna, J.M. Ballesteros, M. Jimenez de Castro, J. Solis, and C.N. Afonso, J. Appl. Phys. 84, 2352 (1998).

[15] M. Benatsou, B. Capoen, M. Bouazaoui, W. Tchana, and J.P. Vilcot, Appl. Phys. Lett. 71, 428 (1997).

[16] A.F. Obaton, J. Bernard, C. Parent, G. LeFlem, J.M. Fernandez-Navarro, J.L. Adam, M.J Myers, G. Boulon, Conf. Digest, OSA Advanced Solid State Laser Conference, p. 335, (1999)

[17] IOG-1 laser glass, Schott Glass Technologies, Inc., 400 York Avenue, Duryea, PA. The IOG-1 trade name is used to allow the reader to reproduce the experiment and does not imply endorsement by the National Institute of Standards and Technology.

[18] Laser Glass: Nd-Doped Glass Spectroscopic and Physical Properties, Lawrence Livermore National Laboratory, M-095, Rev. 2, November 1981.

[19] D.E. McCumber, Phys. Rev. 134, A299, (1964).

[20] W.J. Miniscalo and R.S. Quimby, Optics. Lett. 16, 258 (1991).

[21] D.L. Veasey, K.J. Malone, J.A. Aust, N.A. Sanford, and A. Roshko, Conf. Digest, Proc. 7th Eur. Conf. n Integrated. Optics, p. 579, Delft, (1995), J.E. R man and K.A. Winick, Appl. Phys. Lett. 61, 2744 (1992).

[22] L. Li, M. Xu, G.I. Stegeman, C.T. Seaton, SPIE Proc. 835, 72 (1987)

[23] N. H. Fontaine and M. Young, "Refracted near-field scanning of fibers and waveguides," submitted to Appl. Optics.

[24] D.H. McMahon, W.A. Dyes, J. Lightwave Technol. 6, 1162 (1988).

[25] J.W. Goodman, *Statistical Optics*, Wiley&Sons, 1985, p. 168.

[26] W.H. Loh, B.N. Samson, L. Dong, G.J. Cowle, and K. Hsu, J. Lightwave Technol. 16, 114 (1998).

[27] W.W. Rigrod, J. Appl. Phys. 36, 2487 (1965).

[28] E. Miskovic, Photonics Spectra 33, 105 February (1999).

[29] D.L. Veasey, J.M. Gary, and J. Amin, SPIE Proc. 2996, 109 (1997)

[30] L. Ingber, "Adaptive Simulated Annealing (ASA)," Global optimization C-code, Lester Ingber Research, Chicago, IL (1993). URL http://www.ingber.com/#ASA-CODE

[31]: R.E. Smith, S.N. Houde-Walter and G.W. Forbes, J. Quan.Electron. QE-28, 1520 (1992).

Figure Captions

Fig. 1. Distributed-Bragg-reflector waveguide laser array realized using a single pitch grating and diffused waveguides with varying effective index.

Fig. 2. Schematic of Fabry-Perot waveguide laser test bed

Fig. 3. a) Emission and absorption cross sections as a function of wavelength for Er^{3+} ions in IOG-1 phosphate glass. Spectral emission was calculated using the method of McCumber. b) Emission and absorption cross sections as a function of wavelength for Yb^{3+} ions in IOG-1. $\Delta\lambda_{eff}$ indicates the spectrum width as defined by $\Delta\lambda_{eff} = \int \sigma(\lambda)d\lambda / \sigma(\lambda_{peak})$.

Fig. 4. Refractive index depth profile, measured at 635 nm, of an Er^{3+}/Yb^{3+} phosphate glass waveguide obtained using a refracted near-field scanning method.

Fig. 5. 1540 nm output power as a function of pump power for a 20 mm and a 22 mm long Er^{3+}/Yb^{3+} waveguide lasers. 20 mm long device was pumped at 979 nm and the 22 mm device was pumped at 960 nm. Also shown is a theoretical fit to the data using a waveguide laser model.

Fig. 6. Typical multi-wavelength output spectrum for Fabry-Perot waveguide lasers.

Fig. 7. Extended cavity designs used for tuning of waveguide lasers. a) prism-tuned weakly coupled cavity, b) grating-tuned extended cavity.

Fig. 8. a) tuning curve obtained for grating-tuned Fabry-Perot waveguide laser. Solid lines connect the points as a guide to the eye, b) typical multiwavelength output spectrum of F-P waveguide laser.

Fig. 9. Output power as a function of coupled pump power for a Yb-doped waveguide laser operating at a wavelength of 1.02 μm. The solid line represents the best linear fit to the data from which the slope efficiency was derived.

Fig. 10. Single frequency laser output power at 1536.3 nm as a function of launched 977 nm pump power. The dotted line represents the best linear fit to the data from which the slope efficiency was derived. The inset shows the spectrum of the DBR laser on a linear scale.

Fig. 11. Fabry Perot (FP) interferometer scan of the DBR laser output showing single frequency operation. Inset shows dual frequency operation for pump powers (P_p) exceeding 300 mW. Longitudinal mode spacing is 7.2 GHz, corresponding to an optical cavity length of 1.4 cm.

Fig. 12. Self heterodyne beat spectrum at 75 MHz. The full-width, half-maximum linewidth is approximately 500 kHz.

Fig. 13. a) Relative intensity noise (RIN) in the frequency band from 0.1 to 1.1 GHz using a shot noise calibrated RIN system, b) uncalibrated amplitude noise spectrum showing relaxation oscillation noise peak near 300 kHz. The lower curve represents the noise floor of the measurement system.

Fig. 14. Wavelength of DBR waveguide laser as a function of temperature. Dotted line is for the aid of the eye in following the wavelength trend.

Fig. 15. Simulated laser output power as a function of laser length for several values of output coupler reflectance, b) simulated laser output power as a function of mode-field diameter for a 1-cm long laser cavity.

Fig. 16. Output power as a function of waveguide mode width and height at 1.54 μm and output mirror reflectance for optimized waveguide lasers. Range of output powers in mW is indicated by color bar.

Paper E

Rigorous scalar modeling of Er and Er/Yb-doped waveguide lasers*

David L. Veasey@, John M. Gary, and Jaymin Amin

National Institute of Standards and Technology, Boulder, CO 80303-3328

ABSTRACT

A rigorous scalar model for predicting the characteristics of rare-earth-doped waveguide lasers has been developed. The model consists of two nonhomogeneous wave equations: one for the forward-propagating laser signal power, the other for the backward- propagating laser signal. These equations are coupled with one forward-propagating, nonhomogeneous wave equation representing the pump signal. The three wave equations are coupled with the space dependent laser rate equations to form a system of time dependent differential equations. This large system of equations is solved, using appropriate initial and boundary conditions, by the method of lines using collocation for the spatial approximation. The solutions to this system yield data which predict the time and position-dependent laser signal power, pump power, and population densities in a waveguide laser cavity supporting an arbitrary guided mode. The assumptions made in this new model are that the transverse field maintains the same shape as a function of longitudinal position in the laser cavity and that the effects of spatial hole burning and standing waves are neglected. We have used this model to predict continuous wave and Q-switched laser performance for Er and Er/Yb-doped lasers. We have achieved favorable comparisons with actual laboratory operation of cw Yb/Er-co-doped waveguide lasers. Results from simulations of Er-doped and Yb/Er-doped Q-switched lasers are presented which show that high peak powers on the order of 500 W and 1 ns pulse widths can be achieved.

Keywords: waveguide, laser, Q-switch, erbium, ytterbium, modeling, ion-exchange, sources

2. INTRODUCTION

Over the past several years, there has been considerable interest in the development of solid state waveguide laser sources in dielectric materials such as bulk glasses,[1-6] dielectric films,[7] and electro-optic hosts such as $LiNbO_3$ and $LiTaO_3$.[8-10] The interest in such sources has been motivated primarily by the successful deployment of erbium-doped fiber amplifiers in optical communication systems operating in the 1.55 μm band. Rare-earth-doped glass waveguide lasers offer several advantages over their semiconductor laser counterparts. These advantages include lower manufacturing costs due to relaxed fabrication tolerances over semiconductor lasers, broad wavelength tunability, inherently low relative intensity noise (RIN), and narrower laser linewidths. In addition, the beam profiles and numerical apertures can be nearly exactly matched to optical fibers. They also exhibit high energy storage capacity which is necessary for high-power pulsed operation. One of the primary limitations of planar waveguide devices is that they require short cavity lengths. This means that optically pumped thresholds are somewhat higher than for fiber lasers where the lengths can be arbitrarily extended. In order to overcome this problem, several different approaches can be pursued. One is to increase the doping concentration of the active ion. This increases the gain per unit length of material, thus lowering thresholds. However, when doping concentration is increased, there is a risk in most host materials of concentration quenching. This causes severe performance degradation because of increased cooperative up-conversion.[11] Other solutions for the optimization of waveguide laser sources include optimizing host materials, cavity design (by judiciously choosing cavity lengths and output coupler reflectivities), pump coupling, and the pumping rate (through the introduction of co-dopants such as ytterbium (Yb) with erbium (Er)). It is also very important to carefully design the waveguide index profiles so that they yield ideal mode fields and overlap for the signal and pump waves. In order to achieve ideal performance, one must be careful to do all of the above simultaneously. This exercise is clearly not trivial since one is dealing with a many-parameter, highly nonlinear

---

@ email: veasey@boulder.nist.gov

system. For these reasons, we have developed a laser model to accurately predict waveguide laser performance for continuous wave and pulsed operation modes. This predictive design tool allows us to determine optimum waveguide laser design which will lead to useful, and reliable manufacturable products.

3. THE MODEL FORMULATION

In our model, we have attempted to realistically model a waveguide laser by making as few assumptions as possible while maintaining practical computer run times for the simulation. A picture of a typical waveguide laser and cavity is shown in Figure 1.

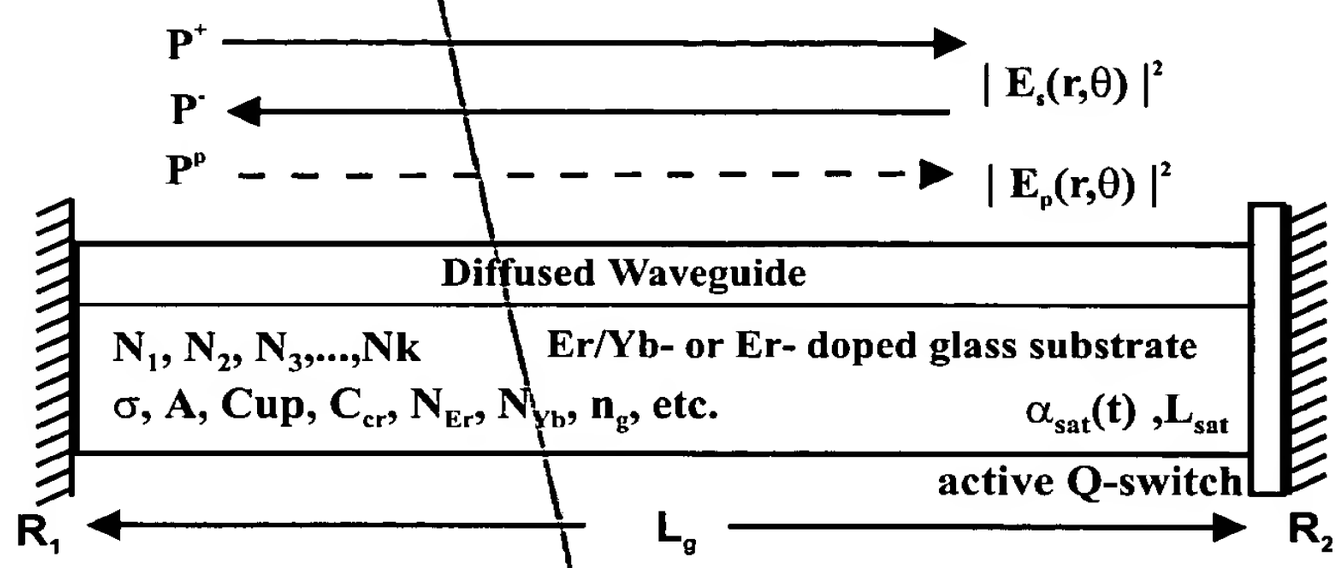

Figure 1. Schematic of laser cavity to be simulated

We have started from basic differential calculus using a semi-classical approach to derive the wave equations which accurately describe propagation in a waveguide laser cavity. A similar derivation of the wave equations was presented by Millonni and Eberly.[12] We also use the semi-classical laser rate equations which are coupled with propagating signals in a laser cavity. The model we have developed for multiple frequencies and a multi-energy level system is described in this section.

The model is grouped into two specific types of equations. These are time dependent scalar wave equations and time/space dependent laser rate equations. The wave equations describe mathematically the forward and backward propagation of the optical frequencies in the laser cavity. For simplicity, we have included only two optical frequencies in the model presented in this paper. These are the laser signal frequency at ł=1542 nm and the pump signal at ł=980 nm. This simplification produces three first order wave equations: one for the forward-propagating laser signal, one for the backward-traveling laser signal, and one for the forward-propagating pump signal. The computer code can accommodate other frequencies simply by adding additional wave equations for each wavelength and direction of propagation.

These wave equations,

$$\frac{\partial P^{+}(z,t)}{\partial t} = -\frac{c}{n_g}\frac{\partial P^{+}(z,t)}{\partial z} + \frac{c}{n_g}\alpha_s(z,t)P^{+}(z,t) + \frac{B_{sp}\int_{\perp} N_2\, dA}{\tau_{21}} \qquad (1)$$

$$\frac{\partial P^{-}(z,t)}{\partial t} = \frac{c}{n_g}\frac{\partial P^{-}(z,t)}{\partial z} + \frac{c}{n_g}\alpha_s(z,t)P^{-}(z,t) + \frac{B_{sp}\int_{\perp} N_2\, dA}{\tau_{21}} \qquad (2)$$

$$\frac{\partial P^{p}(z,t)}{\partial t} = -\frac{c}{n_p}\frac{\partial P^{p}(z,t)}{\partial z} + \frac{c}{n_p}\alpha_p(z,t)P^{p}(z,t) \qquad (3)$$

are coupled with sets of time-dependent laser rate equations, in which the energy level population densities, $N_i = N_i(t,z,r,\theta)$ are functions of time and position. The rate equations are

$$
\left.
\begin{aligned}
\frac{\partial N_1}{\partial t} &= -W_{12}N_1 - W_{13}N_1 + A_{21}N_2 + W_{21}N_2 \\
&\quad + C_{up}N_2^2 - C_{14}N_1N_4 + C_{up3}N_3^2 - C_{cr}N_1N_6, \\
\frac{\partial N_2}{\partial t} &= W_{12}N_1 - W_{21}N_2 - A_{21}N_2 + A_{32}N_3 - 2C_{up}N_2^2 + 2C_{14}N_1N_4, \\
\frac{\partial N_3}{\partial t} &= W_{13}N_1 - A_{32}N_3 + A_{43}N_4 - 2C_{up3}N_3^2 + C_{cr}N_1N_6, \\
N_{Er} &= N_1 + N_2 + N_3 + N_4, \\
\frac{\partial N_5}{\partial t} &= -W_{56}N_1 + A_{65}N_6 + W_{65}N_6 + C_{cr}N_1N_6, \\
N_{Yb} &= N_5 + N_6.
\end{aligned}
\right\} n_0 \, x \, m_0 \qquad (4)
$$

These equations describe the rates at which rare-earth ion energy levels in the material are populated and depleted by absorption, stimulated emission, and spontaneous emission as functions of longitudinal and transverse dimensions. This set of equations was presented by Pasquale. [13] The number of rate equations in a set is determined by the number of energy levels one wishes to track in a simulation. For the Er/Yb-co-doped system in this paper there are six time-dependent equations in a set which means we are tracking six energy levels. There are two time-dependent conservation equations in this system. It is straightforward to alter the rate equation set to account for other interesting energy level transitions. This provides great flexibility for modeling many rare-earth-doped lasers and amplifiers. The transverse dependence of the propagating mode fields is accounted for by sampling a transverse field solution or measured transverse field for a waveguide as a function of two transverse dimensions. At each sample point a set of laser rate equations is introduced into the model to account for the interaction of the transverse field with the stationary ions in the host material.

P^+ and P^- are the forward and backward-propagating laser powers as a function of longitudinal position in the laser cavity. P_p is the forward-propagating pump power in the laser cavity. The pump power, in this case, is assumed to be launched from the end opposite the output coupler which has reflectance, R_2. The optical intensity (in W/cm^2) of the laser signal is $P^{\pm}(z, t) \mid E_s(r, \theta) \mid^2$, where $\mid E_s \mid^2$ is the normalized intensity distribution and has units of cm^{-2}. The pump signal P^p is treated in a similar fashion. The N_i's are the population densities of the various energy levels in the Er/Yb co-doped material. N_1 is the $^4I_{15/2}$ ground state of Er, N_2 is the $^4I_{13/2}$ laser level of Er, N_3 is the $^4I_{11/2}$ 980 nm pump level for Er, N_4 is the $^4I_{9/2}$ 800 nm pump level and upconversion level of Er, N_5 is the $^2F_{7/2}$ ground state of Yb, and N_6 is the $^2F_{5/2}$ pump level of Yb. Figure 2 shows an energy level diagram for the Er/Yb- co-doped system. The Yb pump level is shown as split to illustrate that it has very wide energy range.

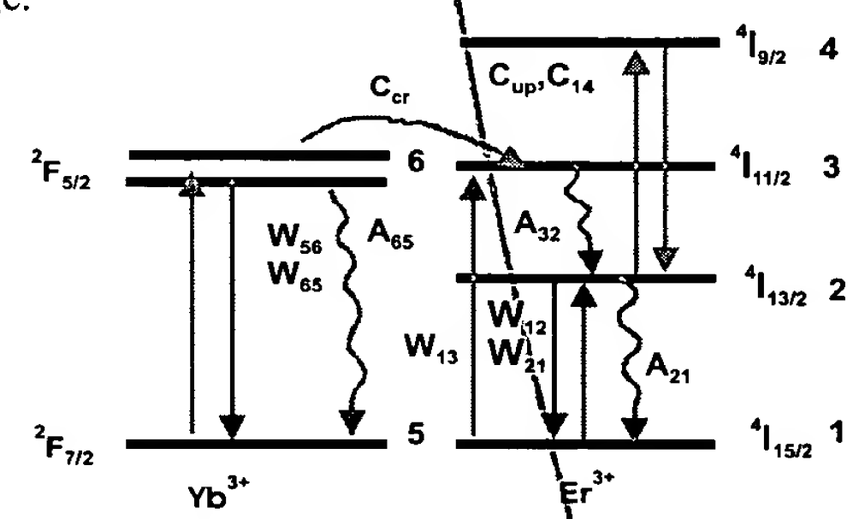

Figure 2. Energy level diagram for Er/Yb-co-doped laser host.

C_{up} is the cooperative upconversion coefficient from the Er $^4I_{13/2}$ laser level, C_{up3} is the cooperative upconversion coefficient from the Er $^4I_{11/2}$ 980 nm pump level, C_{cr} is the cross relaxation coefficient or net forward coupling from the Yb $^2F_{5/2}$ level to

the Er $^4I_{11/2}$ level, and C_{14} is the cooperative down-conversion coefficient or the opposite of cooperative upconversion. The A's are the nonradiative spontaneous emission rates from the first subscript energy level to the second subscript energy level. c is the speed of light in vacuum, n_g is the effective index of the laser mode, n_p is the effective index of the pump mode, and α_s is the gain coefficient as a function of longitudinal position and time inside the laser cavity.

The second term on the right side of equations (1-3) represents the contribution or loss of power in the laser line width due to stimulated emission or absorption and excess waveguide loss at each point z and time t. n_0 x m_0 represents the number of nodes in the transverse dimensions and the two-dimensional grid on which intensities are sampled and on which the N_i's are calculated.

The gain or loss coefficient α_s is computed after Bjarklev[14] by calculating the overlap integral of the normalized propagating power distribution and the population density and then multiplying by the emission or absorption cross sections:

$$\gamma_{21}(z, t) = \sigma_{21} \iint_{\perp} N_2 |E_s|^2 \, dA,$$
$$\gamma_{12}(z, t) = \sigma_{12} \iint_{\perp} N_1 |E_s|^2 \, dA. \tag{5}$$

σ_{21} and σ_{12} are the emission and absorption cross sections of the host material at the laser wavelength. The normalized intensity propagating in the waveguide is assumed to be independent of z, and is normalized by requiring that:

$$\iint_{\perp} |E_s|^2 dA = 1. \tag{6}$$

The gain coefficient as a function of z and t is then given by

$$\alpha_s(z, t) = \gamma_{21}(z, t) - \gamma_{12}(z, t) - \alpha_{is}. \tag{7}$$

α_{is} is the waveguide loss coefficient, which is subtracted to account for excess waveguide losses from scattering and absorption not due to the rare earth ions. It is also possible to add other position dependent losses in this term which are functions of fabrication parameters or cavity configuration. For example, a position and time dependent term can be added to account for mirror losses or localized losses from waveguide loading or for an intracavity coupler.

The pump absorption coefficient α_p is calculated similarly by computing the overlap integral of the ground state populations for the Er ions and the Yb ions with the normalized pump intensity $|E_p|^2$ and multiplying by the pump absorption cross sections, giving:

$$\gamma_{13}(z, t) = \sigma_{13} \iint_{\perp} N_1 |E_p|^2 dA,$$
$$\gamma_{56}(z, t) = \sigma_{56} \iint_{\perp} N_5 |E_p|^2 dA, \tag{8}$$
$$\alpha_p(z, t) = -\gamma_{13}(z, t) - \gamma_{56}(z, t) - \alpha_{ip}.$$

α_{ip} is the excess absorption and scattering loss at the 980 nm pump wavelength. The pump intensity $|E_p|^2$ is normalized in the same way as the signal field, and is written as

$$\iint_{\perp} |E_p|^2 dA = 1. \tag{9}$$

The third term on the right side of equations (1) and (2) represents the contribution of spontaneous emission to the propagating optical power. τ_{21} is the spontaneous emission lifetime of the laser level. The coefficient B_{sp} is given by

$$B_{sp} = \eta c h \upsilon_s, \tag{10}$$

where η is the efficiency of spontaneous emission in the laser line width and is approximated by the ratio of the waveguide

numerical aperture solid angle to the solid angle of a sphere times the integral over frequency of the equivalent spontaneous emission spectrum. $h\upsilon_s$ is the energy of a single laser photon. This approximation of spontaneous emission is similar to the equivalent bandwidth approximation described by Bjarklev.[14]

W_{21}, W_{12}, W_{13} , W_{56}, and W_{65} are the stimulated emission and absorption rates as a function of longitudinal and transverse dimensions and are given by

$$W_{12} = \frac{\sigma_{12}\left(P^+ + P^-\right)\left|E_s\right|^2}{h\upsilon_s}, \quad W_{21} = \frac{\sigma_{21}\left(P^+ + P^-\right)\left|E_s\right|^2}{h\upsilon_s},$$

$$W_{13} = \frac{\sigma_{13}\left(P^p\right)\left|E_p\right|^2}{h\upsilon_p}, \quad W_{56} = \frac{\sigma_{56}\left(P^p\right)\left|E_p\right|^2}{h\upsilon_p}, \tag{11}$$

$$W_{65} = \frac{\sigma_{65}\left(P^p\right)\left|E_p\right|^2}{h\upsilon_p}.$$

We have not included other energy levels in the model as of yet but have plans to add other levels as (outlined by Desurvire [15]) to the Er model. This will allow consideration of excited state absorption (ESA) and its effect on device performance. Each additional energy level adds an extra equation to the rate equation set for each transverse field sample point.

Equations (1)-(4) must be solved simultaneously with appropriate initial conditions and boundary conditions. These conditions determine the laser or amplifier state in which the system will operate. For the laser model, the initial conditions are assumed to be

$$P^+(z,\,0) = P^-(z,\,0) = 0,$$

$$P^p(z,\,0) = P_{R0}\,e^{-\left(\sigma_{13}N_1(z,\,0)+\sigma_{56}N_5(z,0)\right)z}, \tag{12}$$

$$N_1(t=0) = N_{Er}\ ,\ N_{2,3,4}(t=0) = 0,\ N_5(t=0) = N_{Yb},\ N_6(t=0) = 0.$$

These conditions assume that the laser system is initially at rest and that the pump wave has propagated a single cavity length without significantly affecting the population densities in the sample. This is done to avoid sharp discontinuities in the initial condition for the pump.

Boundary conditions are imposed on the values of P^+, P^-, and P^p as follows:

$$P^+(0,\,t) - R_1 P^-(0,\,t) = 0,$$

$$P^-(L,\,t) - R_2\left(e^{2\alpha_{sat}L_{sat}}\right)P^-(L,\,t) = 0, \tag{13}$$

$$P^p(0,\,t) - P_{p0} = 0.$$

R_1 is the reflectance of a highly reflecting mirror at the pump input end of the laser, R_2 is the reflectancd of the output coupler for the laser, and α_{sat} is the time-varying absorption coefficient for an arbitrarily thin absorbing switch placed in the laser cavity just inside of the output coupling mirror. L_{sat} is an effective length of the thin absorber providing the switch with an extinction of $\exp(-\alpha_{sat}L_{sat})$. P_{p0} is the pump power launched at the input end of the sample and held constant from time 0. L is the length of the cavity. For cw operation α_{sat} is set to 0, and for Q-switched operation α_{sat} is set to a function representing the dependence of the absorption coefficient on time. This is an approximate representation of active Q-switching. We could easily make the absorption coefficient of the switch a function of intensity, thus modeling passive Q-switching with a saturable absorber without introducing any more complexity into the model.

4. METHOD OF SOLUTION

At this point our model consists of a large set of coupled integral-differential equations in the form of an initial value problem. The first step in the solution procedure is to transform the integrals so that they can be computed by a generalized Gauss-Laguerre quadrature formula.[16] Using cylindrical coordinates to represent elliptical electrical fields given by

$$\left| E_s \right|^2 = e^{-2\beta_s(\theta)r^2}, \quad \left| E_p \right|^2 = e^{-2\beta_p(\theta)r^2}, \tag{14}$$

the integrals in equation (5) and (8) have the form

$$\int_0^{2\pi}\int_0^{\infty} F(r,\theta)e^{-2\beta(\theta)r^2} r dr d\theta. \tag{15}$$

This integral under the transformation $s=2\beta\theta r^2$, and $\varphi = \theta$, becomes

$$\int_0^{2\pi}\int_0^{\infty} \frac{F(s,\varphi)e^{-s}}{4\beta(\varphi)} ds d\varphi. \tag{16}$$

This is the form required for the use of Gauss-Laguerre quadrature in integration variable *s*.
Once the number n_0 of points, , used to approximate the integrals in *s* is selected, then the location of the points and the corresponding weights for the quadrature are determined by a library routine. [16] Then the integral over *s* is approximated by

$$\frac{2\pi}{m_0}\sum_{k=1}^{m_0}\sum_{j=1}^{n_0} \frac{F(s_j,\varphi_k)}{4\beta(\varphi_k)} w_j. \tag{17}$$

The w_j's are the weights generated by the quadrature routine. The trapezoidal rule is used to approximate the integrals over φ. Thus the problem is discretized over the transverse (s, φ) planes resulting in a hyperbolic initial value problem

$$\frac{\partial \boldsymbol{U}}{\partial t} = f(\boldsymbol{U}, \boldsymbol{U}_z, t). \tag{18}$$

The vector ***U(z,t)*** contains the values of the solution at the discrete points (z_i,s_j,φ_k); that is, $U(t) =(P_i^+, P_i^-, P_i^p, N_{1i,j,k}, \ldots, N_{4i,j,k})$ for $1 \le I \le I_0$, $1 \le j \le n_0$, $1 \le k \le m_0$.

Next, an approximation by cubic Hermite collocation[17] is used to discretize these equations in the z-direction. First a set of nodal points z_i with $z_i < z_{i+1}$ covering the length of the device is selected. The solution is represented by the value of the solution vector ***U*** and its spatial derivatives $\boldsymbol{U}_z$ at each nodal point. These values determine a cubic polynomial in each subinterval (z_i,z_{i+1}). These polynomials are used to approximate the solution. The spatial derivatives, within each interval, are determined by differentiating these polynomials. Instead of representing ***U(z)*** by the values of ***U*** and its derivative at each node, it is convenient to determine the cubic polynomials by the values of ***U(z)*** at two Gaussian quadrature points in each subinterval. In addition the values ***U(0)*** and ***U(L)*** at the endpoints are needed. The Gaussian quadrature points and the endpoints are the collocation points at which the right side of the partial differential equation is evaluated. This results in a system of ordinary differential equations (ODE); that is, a method-of-lines approximation.[18] Finally, the vector of unknowns in the system of ODE's is $W(t) = ((P_v^+, P_v^-, P_v^p, N_{1v,j,k}, \ldots, N_{4v,j,k})$ where the P's approximate the value at the vth collocation point z_v. Here $1 \le n \le 2I_0$, therefore the total number of unknown functions is $(3+n_0m_0)2I_0$. Typical computaions we use have $I_0=10$, $n_0=16$, and $m_0=1$, although we have used m_0 up to 12. This ODE system is solved using a public domain software package by Petzold. [19]

5. CONTINUOUS WAVE LASER RESULTS

We have used this time dependent model to predict the performance of an Er/Yb-co-doped waveguide laser operating in cw mode and Q-switched mode. In both cases the laser is initially assumed to be in a rest state where all of the ions are assumed to be in the ground state and the laser signal powers in the cavity are 0. The pump is turned on at t~0 and is assumed to instantaneously propagate to the other end of the laser cavity without affecting the population inversion. This process in a 2 cm waveguide laser takes approximately 0.1 ns. The solver is started at this point, and the laser cavity powers and energy level populations are tracked as functions of position and time.

For steady state solutions, the code is run until the output power from the laser cavity reaches a steady state. Clearly, this is not the most computationally efficient way to solve for steady state laser performance if that is all we want. Since our primary purpose is to predict time response, we have not yet implemented a more efficient steady state computer code. During the period of below-threshold and above-threshold operation we resolve the time dependent powers in the laser cavity and the variations in population inversions.

Figure 3 shows the predicted steady state output power for a waveguide laser as a function of coupled pump power and as the Yb concentration is increased from 3:1 to 10:1 while leaving the Er concentration constant. All of these simulations were done using 16 transverse nodes in s. Similar results are obtained by using only 7 nodes in the s dimension. Since the solutions for elliptical fields were typically within several percent of those using circular fields, we only used 1 node in φ in order

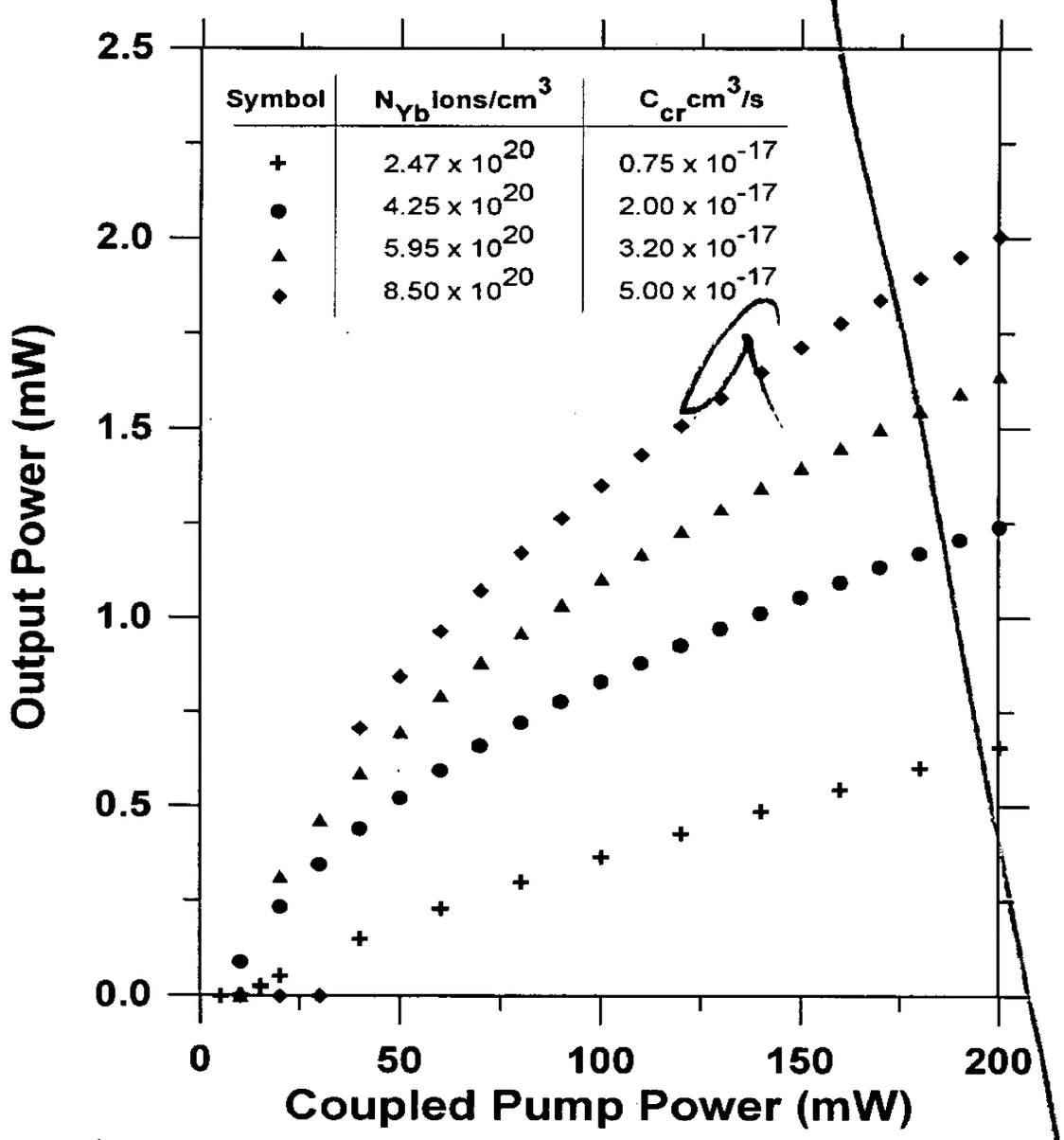

Figure 3. Plot of predicted output power as a function of coupled pump power as the Yb concentration is increased while the Er concentration is constant at $1x10^{20}$ ions/cm^3.

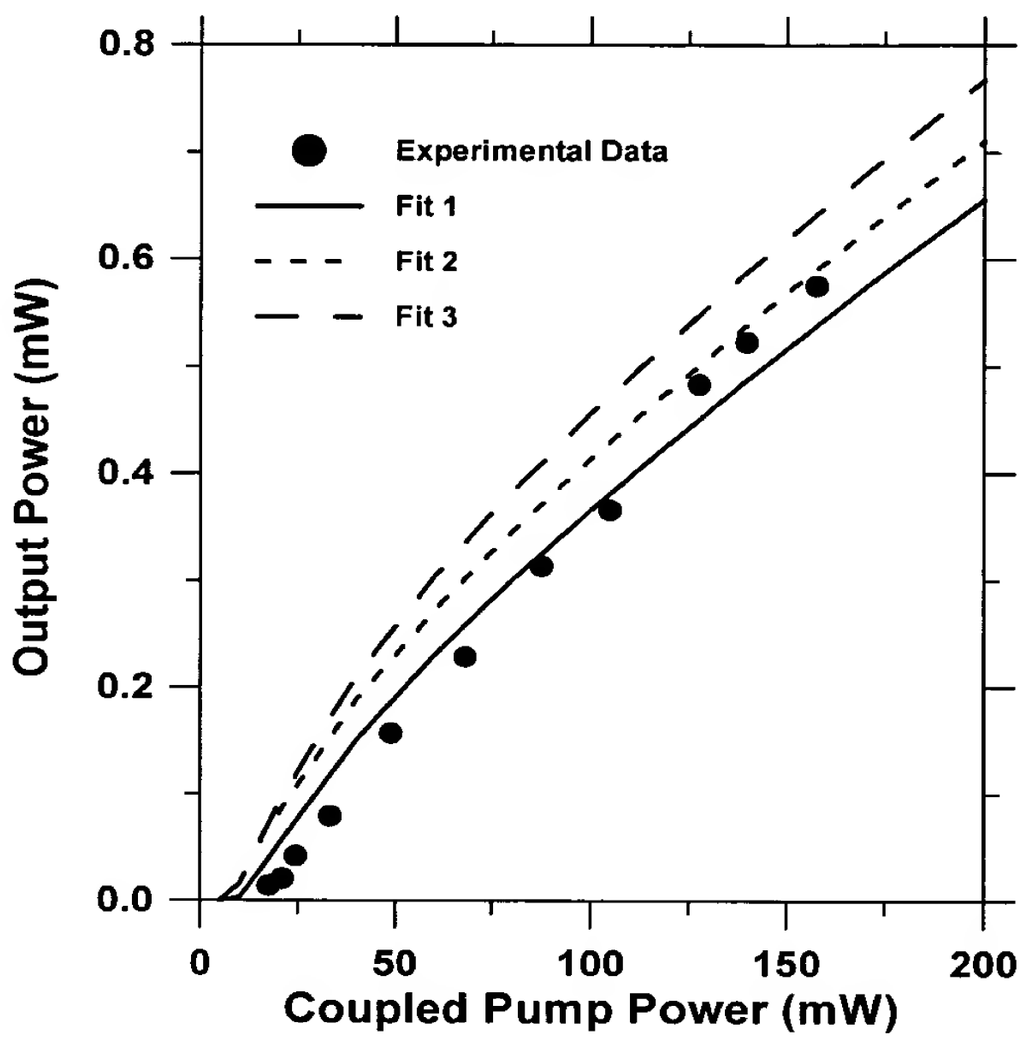

Figure 4. Comparison of theory and experimental data for the Yb/Er co-doped laser. Table 1 lists the bulk of the parameters used in the modeling of the laser device, with the upconversion rate (C_{up}) and the Yb-Er cross relaxation coefficient (C_{cr}) as the variable parameters. For fit 1, C_{up} $=1x10^{-18}$ cm^3/s and $C_{cr}=0.75x10^{-17}$ cm^3/s. For fit 2, $C_{up}=1x10^{-18}$ cm^3/s and $C_{cr}=1x10^{-17}$ cm^3/s. Fit 3 represents $C_{up}=0$ and $C_{cr}=0.75x10^{-17}$ cm^3/s.

to conserve computer time. Table 1 shows the values of the parameters used for these simulations. These parameters are close to those of a phosphorous free alkali-silicate glass which we refer to as NIST-10. Parameters we were not certain of, like the stimulated emission cross sections for the Er/Yb-co-doped material, we obtained by consulting the literature on Yb/Er and Er-doped glasses which are similar in composition to NIST-10. [2,3,11,13,20] Other parameters such as waveguide near field profiles, absorption cross

sections , and lifetimes have been measured and inserted into the model.

It is not instructive to generate a curve like that of Figure 3 for variation in Yb concentration if the cross relaxation coefficient is left constant. This coefficient C_{cr} is a strong function of Yb concentration and increases as the Yb concentration is increased. The primary reason for this increase is that the Yb ions, on average, move closer to the Er ions and thus the transfer efficiency is increased. Discussions of the energy transfer in Er/Yb-co-doped glass are presented by Román et al.[2,21] They present a formula which can be used to determine the cross relaxation coefficients. Upon using this somewhat approximate formula, one finds that for device in Román, the C_{cr} coefficient is approximately 0.5×10^{-17} cm^3/s. This calculation assumes a lifetime of the $^2F_{7/2}$ Yb level to be 2.0 ms and the lifetime of the $^4I_{11/2}$ Er level to be 10 μs. Román also indicates that the efficiency increases as a function of Yb concentration. For the data generated in Figure 3, we have assumed that, as the Yb concentration varies from 2.47×10^{20} ions/cm^3 up to 8.5×10^{20} ions/cm^3, the cross relaxation coefficient increases linearly from 0.75×10^{-17} cm^3/s to 5×10^{-17} cm^3/s. These numbers are close to those deduced from references 2 and 21 for a similar glass composition. We intend to measure these parameters for various concentrations of Yb in the NIST-10 glass in the very near future. If the transfer efficiency is left constant as the Yb concentration is increased, the performance of the lasers is actually degraded slightly due to decreased pumping efficiency for samples of equal length. The laser thresholds increase for higher Yb concentrations. This is due to the fact that, as the Yb concentration is increased, more of the pump is absorbed at the front end of the laser, thus the pumping of the output end of the device is reduced. This has the effect of increasing absorption losses in the laser cavity toward the output end, and thus the thresholds increase. It is clear from the simulation that doping concentration and sample length must be concurrently optimized. The curvature of the power curves is attributed to the gradual saturation of the upper Yb level as the pump power is increased, as reported by Fermann, et al.[22]

We have demonstrated laser operation in several NIST-10 waveguide samples doped with Er and with Er/Yb. The waveguides were prepared by molten salt ion-exchange. Details of the process will follow in subsequent publications. Figure 4 shows a comparison of laboratory data with the predictions obtained from the simulation. To generate these theoretical curves, we used the Yb-Er cross relaxation coefficient C_{cr} and the uniform upconversion coefficient C_{up} as fitting parameters since these spectroscopic parameters have not yet been determined in a systematic way for our glass. The values we used for the fits are indicated on Figure 4 and typify values quoted in the literature for dopant concentrations used in the NIST-10 silicate glass.[2,3,11,13,20] For all of the fits, the waveguide excess loss at the 1542 nm laser signal wavelength was set at 0.15 dB/cm, which was slightly lower than the measured value of 0.2 dB/cm at 1300 nm. The excess loss at the pump wavelength was set at 0.3 dB/cm. These values represent what we think are realistic loss values for the pump and signal fields, given the values measured by the cut-back method at 1300 nm. Fit 1, represented by the solid line, is the closest of the three fits to slope efficiency and threshold, and we think that it falls within our experimental error. However, the error in our power measurements has not yet been fully characterized. Fit 2 shows the effect of increasing the cross relaxation coefficient slightly from 0.75×10^{-17} cm^3/s to 1.0×10^{-17} cm^3/s while the upconversion rate is held constant. This small change has the effect of increasing the output power of the laser due to increased pumping efficiency, however, the threshold is not changed significantly. This is most likely due to the low propagation losses in the waveguides. Fit 3 shows the effect of eliminating uniform upconversion from the simulation while maintaining the cross relaxation coefficient at its original value of 0.75×10^{-17} cm^3/s. The effect of this is to increase the laser output power by a small amount, thus showing that the low upconversion rate used in the model does not significantly deteriorate performance.

Figure 5 is a plot which shows how the slope efficiency and the threshold of this laser will vary as a function of the output coupler reflectivity. The experimental laser characteristics shown in Figure 4 are for an output coupler reflectivity of 98 percent. This operating point is marked on Figure 5 by the circled diamond. This operating point is good for low threshold operation, but is a poor for high output power. Note that this is a poor operation point if high output power is desired, but is a point of lower laser threshold. A good compromise between output power and threshold would be to adjust the output coupler from 98 percent reflectance to 75 percent. This would increase the slope efficiency nearly four times while only doubling the threshold. This is an excellent illustration of the necessity for an accurate laser model, in that it allows for rapid design convergence for optimized rare-earth-doped waveguide lasers.

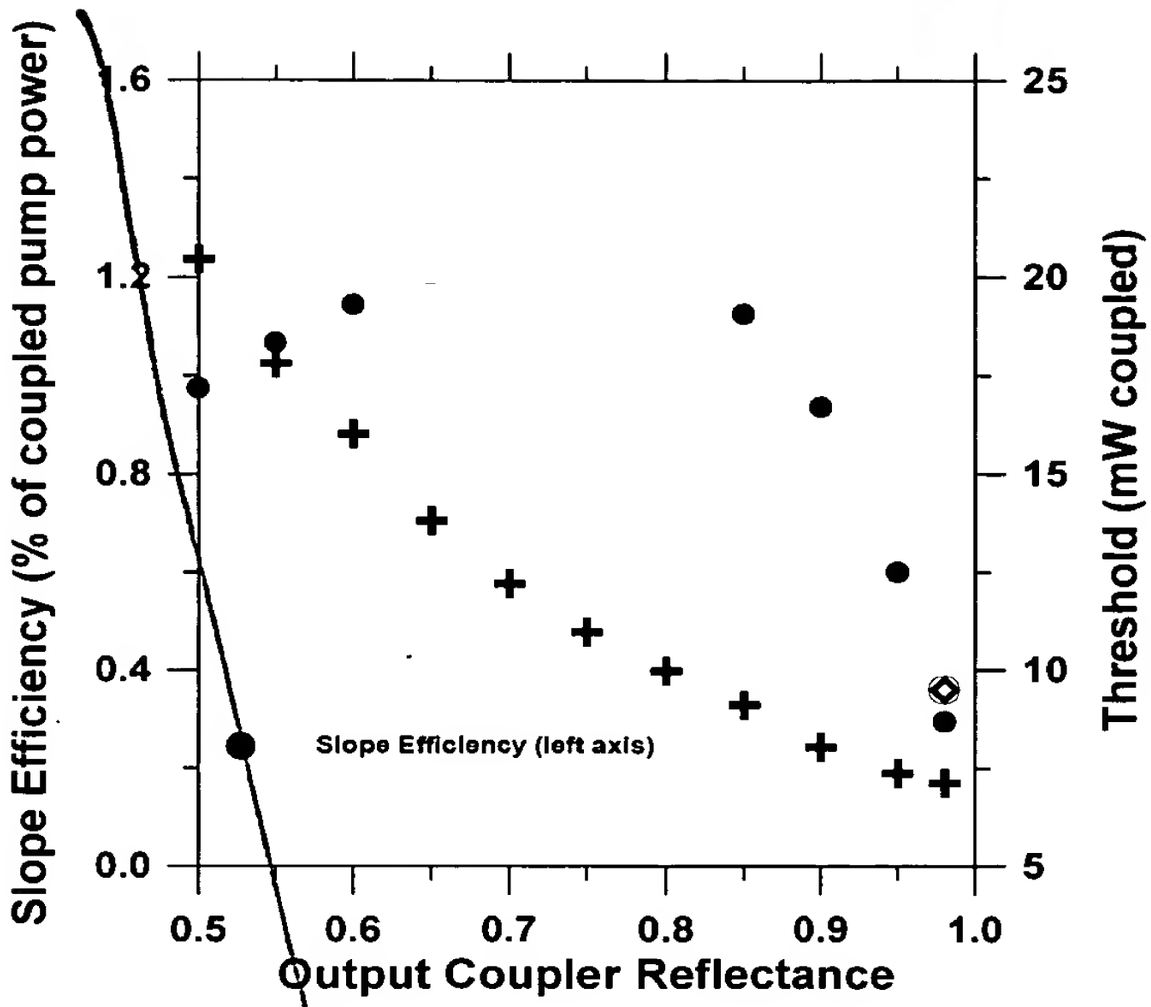

Figure 5. Plot showing the dependence of the laser slope efficiency (left axis) and the laser threshold (right axis) as a function of the cavity output reflectance R_2. The slope efficiency of the laboratory demonstration of the device is marked by the circled diamond.

6. Q-SWITCHED LASER SIMULATIONS

Finally, we have used the time-dependent laser simulation to model a Q-switched waveguide laser. We have used the cavity configuration of Figure 1, in which the Q-switch is an active switch which is mounted onto the end of a waveguide facet. An integrated mirror is deposited on the back side of the switch material. Such a switch is possible using a semiconductor multi-quantum-well structure. Again, the simulation is run with the laser system starting at rest but with the Q-switch closed or in the high absorption state. This allows the pump to rapidly create a population inversion which is well above threshold for the laser when the Q-switch is opened. We have programmed the active Q-switch to open in 5 ns using a cosine s-bend function. The initial extinction was set at α_s = -50, which holds the laser well below threshold with L_{sat}=0.5 mm. The coupled pump power was set to 200 mW and the system was pumped for 2 ms before the switch was opened. What makes our model unique from other Q-switch models is that we have not assumed that we have a high-Q cavity or a uniform intensity in the cavity. We have not assumed a plane wave electric field, we include several levels and transitions instead of the typical two or three, and we track the saturation of the pumping intensity. In addition, we do not assume that the distribution of energy level population densities assumes the same shape as the pump or the signal field. The populations are allowed to vary freely as functions of position and intensities.

Figure 6 is a family of Q-switch pulse simulations using the same parameters that were used in Fit 1 of Figure 4. These simulations varied only the output coupler reflectance. As the reflectance is decreased, a more nearly optimal point for the extraction of power is reached and the pulses narrow slightly and have higher peak powers. The optimum for this cavity length is approximately 80 percent reflectance, resulting in a peak power prediction of 346 W. If the reflectivity is decreased beyond this point, the round trip gain of the cavity coupled with the average lifetime of a photon in the laser cavity causes the pulses to widen and have less peak power. We have not yet determined the primary factor that determines pulse width. We have found that many parameters are involved in pulse width determination. We have shown that the peak pulse power can be optimized further by decreasing the cavity length from 2 cm to 1.4 cm. At this point, the optimum pulse is slightly narrower in width and the simulated peak power is over 400 W. Other important parameters which affect the pulses, such as near field size, signal-pump overlap, Yb-doping concentration, and Er-doping concentration, are being investigated.

7. SUMMARY

In summary, we have presented a detailed time dependent model for use in the simulation of integrated photonic waveguide lasers. The model treats the waveguide laser with very few approximations. Approximations which we do make are those concerned with the tracking of signal and pump phase. We do not track the phases of waves propagating in the laser cavity. This prohibits us from predicting effects such as cavity standing waves and spatial hole burning, and the dependence of the population densities and

intensities related to these effects.

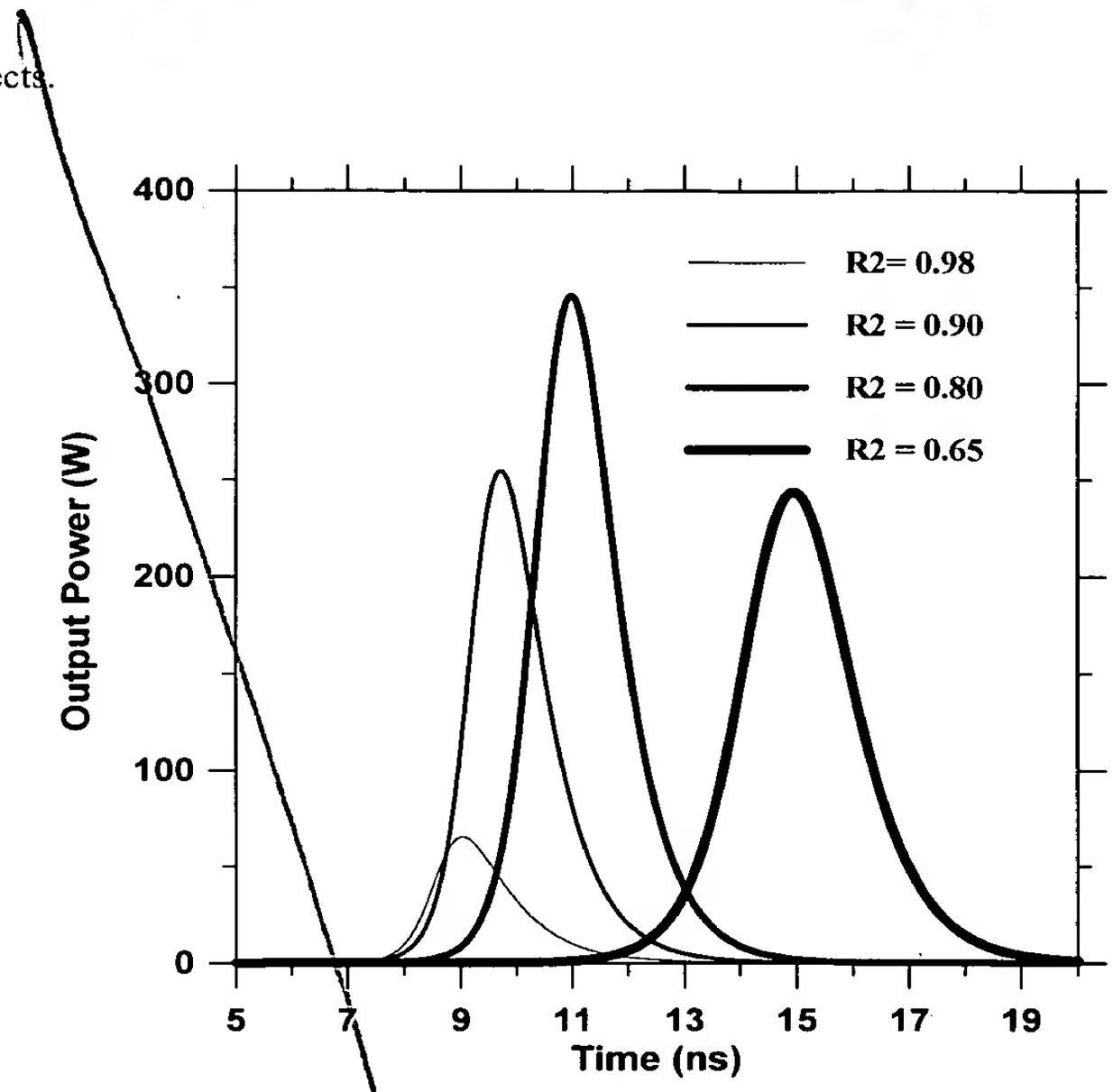

Figure 6. Prediction of Q-switch pulses from the demonstrated Er/Yb-co-doped waveguide laser. The reflectance of the output coupler is varied from 98 percent to 65 percent. The graph shows that the optimum pulse (highest peak power and small width) is extracted when the reflectance is optimized to 80%. The FWHM pulse width for the $R_2 = 98\%$ pulse is 1.58 ns, the $R_2 = 90\%$ pulse width is 1.5 ns, the $R_2 = 80\%$ pulse width is 1.68 ns, and the $R_2 = 65\%$ pulse width is 2.32 ns.

Other approximations we make are that the intensity distributions in the waveguide do not vary as functions of z or time and spontaneous emission is not discretized into many frequencies. The model in its present form, gives us the capability to accurately model waveguide lasers and amplifiers. We have successfully used the model in a predictive fashion to simulate laboratory results for continuous wave Yb/Er co-doped waveguide lasers. The fits from the simulation to the slope efficiency data are excellent using realistic values for all of the pertinent input parameters.

In addition, we have reported the predicted Q-switched performance of Er/Yb-co-doped glass waveguide lasers and have shown that values of peak power can reach hundreds of watts for sample lengths of the order of 1-2 cm. These simulations have used parameters for fabricated waveguide lasers. We have not sufficiently investigated the design space and we strongly believe that more optimum designs can be achieved. An exhaustive investigation of the design space and the interplay among laser parameters is currently underway. Simulations not discussed here suggest that powers on the order of 1 kW can be achieved through the optimization of cavity design and the careful engineering of waveguide index profiles to maximize overlap of the pump and signal guided waves.

We anticipate that this model will be used extensively to model several different rare earth systems for laser and amplifier performance. This work will be done in order to optimize the designs of waveguide and fiber lasers and also to determine the most critical host parameters. In this way, the model acts as a metrology tool by indicating which parameters have the greatest effect on laser performance. These parameters can then be measured more accurately to facilitate the development of more suitable host materials. These simulations have proven to be an invaluable tool for our current work in rare-earth-doped materials and devices.

ACKNOWLEDGEMENTS

The authors thank Bradley Alpert of NIST for helpful discussions and for the provision of several computer codes which greatly benefited the development of the equation solver.

REFERENCES

1. T. Feuchter, E.K. Mwarania, J. Wang, L. Reekie, and J.S. Wilkinson, "Erbium-doped ion-exchanged waveguide lasers in BK-7 glass," *IEEE Photonics Technology Letters*, **4**, pp. 542-544 (1992).
2. J.E. Román, M. Hempstead, W.S. Brockleby, S. Nouh, J.S. Wilkinson, P. Camy, C. Lerminiaux, and A. Béguin, " Ion-exchanged Er/Yb waveguide laser at 1.5 μm pumped by a laser diode," *Electronics Letters,* **31**, pp. 1345-1346 (1995).
3. G.L. Vossler, C.J. Brooks, and K.A. Winick, "Planar Er:Yb glass ion exchanged waveguide laser," E*lectronics Letters*, **31**, pp. 1162-1163 (1995).
4. D. Barbier, J.M. Delavaux, R.L. Hyde, J.M. Jouanno, A. Kervorkian, and P. Gastaldo, "Tunability of Yb/Er integrated optical lasers in phosphate glass," *Proceeding of Optical Amplifiers and their Applications*, postdeadline paper PD3 (Davos, 1995).
5. D.L. Veasey, K.J. Malone, J.A. Aust, N.A. Sanford, and A. Roshko, " Distributed feedback lasers in rare-earth-doped phosphate glass," Proceedings of the 7th European Conference on Integrated Optics (Delft, 1995).
6. J.A. Aust, K.J. Malone, D.L. Veasey, and N.A. Sanford, "Passively Q-switched Nd-doped waveguide laser," *Optics Letters*, **19**, pp. 1849-1851 (1994).
7. T. Kitagawa, K. Hattori, M. Shimizu, Y. Ohmori, and M. Kobayashi, "Guide-wave laser based on erbium-doped silica planar lightwave circuit," *Electronics Letters*, **27**, pp. 334-335 (1991).
8. J.Amin, J.A. Aust, and N.A. Sanford, " Z-propagating waveguide lasers in rare-earth-doped Ti:$LiNbO_3$," *Applied Physics Letters*, **69**, pp. 3785-3787 (1996).
9. I. Baumann, R. Brinkmann, M. Dinand, W. Sohler, and S. Westhöfer, "Ti:Er:$LiNbO_3$ waveguide laser of optimized efficiency," IEEE Journal of Quantum Electronics, **32**, pp. 1695-1706 (1996).
10. N.A. Sanford, J.A. Aust, K.J. Malone, and D.R. Larson, "Nd:$LiTaO_3$ waveguide laser," Optics Letters, **17**, pp. 1578-1580 (1992).
11. M. Federighi and F. Di Pasquale, " The effect of pair-induced energy transfer on the performance of silica waveguide amplifiers with high Er^{3+}/Yb^{3+} concentrations," *IEEE Photonics Technology Letters*, **7**, pp. 303-305 (1995).
12. P.W. Milonni and J.H. Eberly, *Laser,* New York, Wiley, 1988, ch. 10.
13. F. Di Pasquale and M. Federighi, "Improved Gain Characteristics in High-Concentration Er^{3+}/Yb^{3+} Co-doped Glass Waveguide Amplifiers," *IEEE Journal of Quantum Electronics*, **30**, pp. 2127-2131 (1994).
14. A. Bjarklev, *Optical Fiber Amplifiers: Design and System Applications,* Artech House, Boston-London, ch 5, (1993).
15. E. Desurvire, *Erbium-doped Fiber Amplifiers*, Wiley, New York, p. 278 (1994).
16. G. Golub and J. Welsch, "Calculation of Gauss Quadrature Rules," *Math Comp*, **23** , pp. 221-230 (1969).
17. M. Schultz, *Spline Analysis* , Prentice Hall, Englewood Cliffs, N.J. (1973).
18. M. Davis, *Numerical Methods and Modeling for Chemical Engineers*, Wiley, New York (1984).
19. Petzold, "A description of DASSL: A Differential/Algebraic System Solver," *Proc. IMACS World Congress*, Montreal, Canada (1982).
20. J.E. Roman, M. Hempstead, C. Ye, S. Nouh, P. Camy, P. Laborde, and C. Lerminiaux, "1.7 μm excited state absorption measurement in erbium-doped glasses," *Applied Physics Letters*, **64**, pp. 470-472 (1995).
21. J.E. Román, M. Hempstead, W.S. Brocklesby, S. Nouh, J.S. Wilkinson, P. Camy, C. Lerminiaux, and A. Béguin, "Diode pumped, ion-exchanged Er/Yb waveguide laser at 1.5 μm in phosphorous-free silicate glass," Proc. 7th European Conf. on Integrated Optics, postdeadline paper, pp. 13-16 (Delft 1995).
22. M.E. Fermann, D.C. Hanna, D.P. Shepherd, P.J. Suni, and J.E. Townsend, "Efficient operation of an Yb-sensitized Er fibre laser at 1.56 μm," *Electronics Letters*," **24**, pp. 1135-1136 (1988).

Table 1. Parameters used to model the Er/Yb co-doped waveguide laser

Length of Waveguide Laser Cavity	L = 2 cm
Signal Field Width (circular gaussian, 1/*e* FW)	$W_s = 3.75 \times 10^{-4}$ cm
Pump Field Width (circular gaussian, 1/*e* FW)	$W_p = 2.40 \times 10^{-4}$ cm
Signal Effective Index	$n_s = 1.53$
Pump Effective Index	$n_p = 1.53$
Spontaneous Emission Lifetime of $^4I_{13/2}$	$\tau_{21} = 11$ ms $= 1/A_{21}$
Stimulated Emission Cross Section 1542 nm ($^4I_{13/2}$-$^4I_{15/2}$)	$\sigma_{21} = 6.3 \times 10^{-21}$ cm^2
Peak Absorption Cross Section 1542 nm ($^4I_{15/2}$-$^4I_{13/2}$)	$\sigma_{12} = 5.7 \times 10^{-21}$ cm^2
Er Pump Absorption Cross Section 980 nm ($^4I_{15/2}$-$^4I_{11/2}$)	$\sigma_{13} = 1.1 \times 10^{-21}$ cm^2
Yb Absorption Cross Section 980 nm ($^2F_{7/2}$-$^2F_{5/2}$)	$\sigma_{56} = 8.2 \times 10^{-21}$ cm^2
Yb Emission Cross Section 980 nm ($^2F_{5/2}$-$^2F_{7/2}$)	$\sigma_{65} = 11.9 \times 10^{-21}$ cm^2
Yb-Er Cross Coupling Coefficient C_{cr}	Fitting parameter, see text
Upconversion Coefficient C_{up}	Fitting parameter, see text
Signal Wavelength	$\lambda_s = 1542$ nm
Pump Wavelength	$\lambda_p = 974$ nm
Er Ion Density	$N_{er} = 0.85 \times 10^{20}$ cm^{-3}
Yb Ion Density	$N_{yb} = 2.47 \times 10^{20}$ cm^{-3}
High Reflector Reflectance	$R_1 = 0.995$
Output Coupler Reflectance	$R_2 = 0.98$
Nonradiative Lifetime of Level $^4I_{11/2}$	$\tau_{32} = 10$ ms $= 1/A_{32}$
Excess Waveguide Scattering Loss	$\alpha_{is} = 0.15$ dB/cm $\alpha_{ip} = 0.3$ dB/cm